DE GRUYTER DOI 10.1515/nanoph-2013-0021 — Nanophotonics 2014; 3(4-5): 283–311

Review article

Daoxin Dai* and John E. Bowers

Silicon-based on-chip multiplexing technologies and devices for Peta-bit optical interconnects

Abstract: An effective solution to enhance the capacity of an optical-interconnect link is utilizing advanced multiplexing technologies, like wavelength-division-multiplexing (WDM), polarization-division multiplexing (PDM), spatial-division multiplexing (SDM), bi-directional multiplexing, etc. On-chip (de)multiplexers are necessary as key components for realizing these multiplexing systems and they are desired to have small footprints due to the limited physical space for on-chip optical interconnects. As silicon photonics has provided a very attractive platform to build ultrasmall photonic integrated devices with CMOS-compatible processes, in this paper we focus on the discussion of silicon-based (de)multiplexers, including WDM filters, PDM devices, and SDM devices. The demand of devices to realize a hybrid multiplexing technology (combining WDM, PDM and SDM) as well as a bidirectional multiplexing technologies are also discussed to achieve Peta-bit optical interconnects.

Keywords: wavelength-division-multiplexing (WDM); polarization-division multiplexing (PDM); spatial-division multiplexing (SDM); hybrid multiplexing; bidirectional multiplexing; silicon; Peta-bit; photonic integrated circuit (PIC).

***Corresponding author: Daoxin Dai,** Centre for Optical and Electromagnetic Research, State Key Laboratory for Modern Optical Instrumentation, Zhejiang University, Zijingang, Hangzhou 310058, China, e-mail: dxdai@zju.edu.cn
John E. Bowers: Department of Electrical and Computer Engineering, University of California, Santa Barbara, CA 93106, USA

Edited by Chris Doerr

1 Introduction

Modern micro-processors include tens to hundreds of cores on a single die to improve performance. In order to maximize their performance, a very large bandwidth is needed for the cores to access data stored in local and distant caches as well as in off-chip main memory [1, 2]. For example, the required bandwidth for a Corona architecture consisting of 256 cores with a goal of 10 TFLOP peak performance, is 10 TBps when one byte per FLOP for on-/off-chip communication is used [3]. To meet such a bandwidth challenge for communication among the cores and off-chip memory, optical interconnects are regarded as a very promising solution by combining monolithic CMOS silicon photonics and optimized processor-memory network architectures [1, 2]. If we take into account the core number will continue to increase to more than 1000 in the following years as many industry pundits predict, the capacity of an optical-interconnect link must be improved further [3]. An effective solution is utilizing advanced multiplexing technologies [3], including wavelength-division-multiplexing (WDM), polarization-division multiplexing (PDM), spatial-division multiplexing (SDM), etc, as are used for long-haul optical fiber communications.

For example, DWDM (dense WDM) technology has been used very widely to enable tens of channels with different carrier wavelengths to transmit along a single mode optical fiber for long-haul networks. A natural evolution is to extend this technology to data centers [2]. However, in a DWDM system the emission wavelengths of all the laser sources have to be aligned and stabilized precisely by e.g., controlling the temperature of the chip carefully. As a consequence, the management for wavelength tuning, conversion, routing and switching in DWDM systems becomes complicated, expensive, and power-hungry, which is acceptable for the long-haul optical network. For on-chip optical networks, however, it might be too expensive and power-consuming to afford especially when lots of laser sources and drivers are included on one chip. As a result, regarding to the realization of affordable intra-chip / inter-chip optical interconnects with low-power-consumption, CWDM (coarse WDM) technology is a potentially better option than DWDM technology regarding to the relaxed requirements for the wavelength alignment/control. A 4-channel CWDM link with 400 GHz channel-spacing has been used to realize a 50 Gbps communication link between two chips [4]. The short transmission distance means the transparent window for optical waveguides or fibers is large, which makes more CWDM channels available if needed. Recent progress of CWDM devices will be reviewed in Section 2.

It is also interesting and necessary to enhance the link capacity with single-wavelength carrier light. In this case, the technologies of polarization-division multiplexing (PDM) and space-division multiplexing (SDM) become very useful. PDM technology has been used to enhance the capacity for long-haul optical fiber communications by utilizing two orthogonal polarizations together with phase modulation or optical quadrature amplitude modulation (QAM), which allows transmission speeds of 100 Gbit/s or more over a single wavelength [5]. Due to the random variation of the polarization state of light in fibers, PDM is generally used together with advanced channel coding techniques so that digital signal processing (DSP) can be used to decode the signal. Note that the polarization state of light can be maintained very well for the case of on-chip optical interconnects since optical signals propagate along highly birefringent planar optical waveguides within the chip. Therefore, it is not necessary to work with advanced channel coding techniques as well as DSP so that the PDM for on-chip optical interconnects can be simplified. In Section 3, we give a review for polarization handling devices used to realize PDM technology.

SDM technology provides a way to improve the capacity by using multi-core [6] or multimode optical waveguides/fibers [7, 8], and has attracted more and more attention for long-haul optical fiber communications in the recent years. When using multi-core SDM technology for photonic networks-on-chip, the advantage is that the links are separated physically and no (de)MUXer is needed. The drawback is the large footprint and the increased layout complexity especially when there are many waveguide cores included. For example, a significant excess loss might be introduced due to the waveguide crossings, which usually exists for large-scale photonic integrated circuits (PICs). And it is not convenient to switch optical signals between any two waveguides due to the limited physical space. An alternative is using multimode SDM technology [9–11], for which each eigen-mode in a multimode optical waveguide carries different data. Multimode SDM has been proposed to enhance the capacity of fiber optical communications [7]. However, it is not easy to achieve mode (de)Muxer to handle higher-order modes in a multimode optical fiber. Recently multimode SDM technology has been developed very well with a few-mode fiber which only supports a few modes. Some complicated free-space optical setups are introduced for mode (de)multiplexing [8], which, however, is very difficult to extend for having more modes included. One should note that the situation becomes much better for photonic networks-on-chip because optical signal propagates along planar optical waveguides within chips, in which case the eigen-modes could be converted conveniently by using some specific PICs [10]. This makes it very attractive to develop multimode SDM technology for on-chip optical networks. Recent progresses on devices for mode (de)multiplexing technology are reviewed in Section 4.

In order to improve the total capacity to be up to Peta-bit/s, a potential way is combining all these multiplexing technologies to form a kind of multi-dimensional hybrid multiplexing technology, which will be discussed in Section 5.1. Bidirectional multiplexing technology can be usually applied to establish the optical interconnects between two chips, for which non-reciprocal devices are needed. This will be discussed in Section 5.2.

Regarding that silicon photonics has provided a very attractive platform to build ultrasmall integrated photonic devices with standard CMOS (complementary metal oxide semiconductor) processes, this paper will review recent progresses of the key photonic integrated devices on silicon for realizing the multiplexing technologies used in photonic networks-on-chip.

2 Silicon-based WDM filters

Utilizing the interference of optical beams provides a fundamental principle to realize wavelength-selective response desired for WDM filters. It is well known that a Mach-Zehnder interferometer (MZI) is a basic device with two-beam interference and a single-stage MZI has a sine-like spectral response. An improved spectral response can be synthesized with multiple cascaded MZIs by optimizing and controlling the coupling coefficients as well as the critical phase delays of the stages [12]. For example, a cascaded MZI filter with flattened spectral responses can be achieved, which is useful for two-channel optical interleavers [13–16]; however, it is still not easy to achieve multi-channel WDM (de)multiplexers by using MZIs. Alternatively, multi-beam interference is preferred because it enables narrow-passband wavelength filtering over a large wavelength period (i.e., the free spectral range, FSR). The typical multi-beam interferometers include arrayed-waveguide gratings (AWGs) [17–29] and echelle diffraction gratings (EDG) [30–34], which can (de)multiplex tens of WDM channels simultaneously and have been used in practical DWDM systems worldwide. In Section 2.1, we give a review for recent progresses on these two types of planar waveguide (de)multiplexers (i.e., AWGs as well as EDGs) with ultrasmall footprints based on silicon-on-insulator (SOI) nanowires.

Another form of multi-beam interferometer is based on optical cavities (e.g., F-P cavities, microring resonators (MRRs), etc) [35–38], which have periodical Lorentzian spectral responses to select a series of resonance wavelengths. For WDM applications, in order to select one or several channels from all channels multiplexed, one can choose one or more optical cavities and each cavity should be designed to have a FSR large enough to cover all the multiplexed channels. When using an F-P cavity (which is a standing-wave resonator with two ports), one channel is dropped from the output ports while the other channels are reflected back to the input port. Consequently it is not suitable to use F-P cavities for multi-channel demultiplexing. In contrast, an MRR is a travelling-wave resonator with two or four ports and there is no reflection ideally. It is convenient to cascade many MRRs and even realize an array with N×N elements to deal with N channels [39]. We will discuss MRR filters in Section 2.2.

2.1 Planar waveguide (de)multiplexer (AWGs & EDGs)

2.1.1 AWGs

An AWG consists of input waveguides, arrayed waveguides, output waveguides as well as one or two free propagation regions (FPRs) [17]. The adjacent arrayed waveguides have a constant length difference ΔL, which is an important parameter to influence the dispersion ability of an AWG [18]

$$\Delta L=(\lambda_0 n_s d_g D)/(\Delta\lambda_{ch} N_g R),$$

$$n_g \Delta L=m\lambda_0,$$

where λ_0 is the operation wavelength, $\Delta\lambda_{ch}$ is the channel spacing, n_s is the effective index of the FPR slab waveguide, n_g and N_g are respectively the effective index and the group index of the arrayed waveguide, d_g is the end separation of the arrayed waveguides, D is the separation of the output waveguides, R is the FPR length, and m is the interference order.

AWG (de)multiplexers have been commercialized with low-index-contrast optical waveguides, e.g., SiO_2-on-Si buried waveguides [40, 41]. However, the AWG chip usually has a size of several cm^2. Instead very small AWG (de)multiplexers can be realized when using SOI nanowires with ultra-high Δ and ultrasmall cross section [19–26]. However, the performance (especially the crosstalk) of SOI-nanowire AWGs is very sensitive to the size variation of the arrayed waveguides (e.g., the non-uniformity of the Si-core dimension) [23]. With the current fabrication technologies, the roughness for the core sidewall of SOI nanowires is about 2 nm [16] and the fluctuation due to this core-width variation can be reduced by enlarging the core width in the straight regions [23]. Note that the top silicon thickness uniformity of 6-inch SOI wafers is about ±2 nm and the uniformity is improved to about ±1 nm in a area as small as 1 mm^2 [42, 43]. Therefore, it is helpful to minimize the phase error if the AWG/EDG occupies a small area.

It is well known that ultrasmall bending radius (R~2 μm) and decoupling separation (~2 μm) are allowed for SOI nanowires [44], which is very helpful to reduce the AWG size. However, when using a standard AWG layout design, the separation between two adjacent arrayed waveguides may be much larger than the decoupling separation (~2 μm [44]) of SOI-nanowire waveguides to achieve the length difference ΔL between adjacent arrayed waveguides as required. Therefore, the layer design of an SOI-nanowire AWG should be improved to minimize the footprint. We proposed several kinds of novel layouts with overlapped FPRs [45], microbends as well as spirals in the arrayed waveguides [46, 47]. A reflective AWG demultiplexer with photonic crystal (PhC) reflectors was also demonstrated in order to reduce the AWG size further and make the layout design of AWGs very flexible.

A. Ultrasmall AWG (de)multiplexer with overlapped FPRs

Figure 1A shows the picture of a fabricated AWG (de) multiplexers with two overlapped FPRs [22]. Each half of an arrayed waveguide includes three straight waveguides which are connected smoothly by two bending waveguides in sequences. With such a layout, the structure becomes more compact than a conventional one. We have designed and fabricated a 5×5 SOI-nanowire AWG (de)multiplexer with ultrasmall footprint of only ~40 μm×~50 μm, as shown in Figure 1A. In this design, the total number of arrayed waveguides N_{WG}=12, the channel spacing $\Delta\lambda_{ch}$=11 nm. Figure 1B shows the measured spectral responses of all the five channels for TE polarization. It can be seen that the device has a relatively low crosstalk (~-17 dB) and uniform responses.

B. AWG (de)multiplexer with micro-bends

Figure 2A and B shows the fabricated AWG with a novel layout including overlapped FPRs and arrayed waveguides with a series of microbends. These microbends enable a large lightpath difference in a small

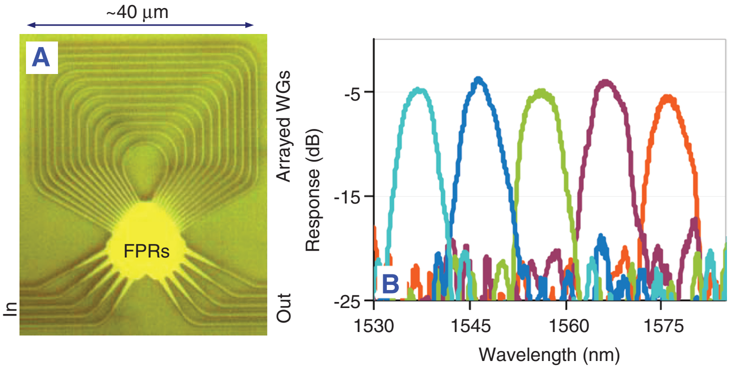

Figure 1 (A) Picture of the fabricated AWG (de)multiplexers with two overlapped FPRs; (B) the measured spectral responses for all five channels.

occupied area (with a small separation between waveguides), and consequently the total size is minimized. The demonstrated 400 GHz 15×15 AWG router has 34 arrayed waveguides and the total size is only 163 μm×147 μm. Figure 2C shows the measured spectral responses of 15 channels when the TE polarization light is input from the central input waveguide. The channel spacing is around 3.1 nm, which is close to the design value 3.2 nm. The crosstalk between adjacent channels is ~–10 dB, which is partially due to the phase errors in the arrayed waveguides with microbends. The temperature dependence for the AWG router was also characterized. Figure 3A shows the measured spectral response of the central output channel as the temperature varies form 23°C to 110°C. It can be seen that the channel wavelength can be thermally tuned effectively and the temperature dependence of the central wavelength is about 0.068 nm/°C.

C. Reflective-type AWG (de)multiplexer

Another effective method to reduce the size of an AWG is using a reflective-type structure [48–50]. However, the layout design freedom for those conventional reflective-type AWG based on micrometric optical waveguides is limited. First, the sections at the end of arrayed waveguides are arranged in parallel and they are perpendicular to the same reflection mirror [48–50]. Second, one usually has to cleave or dice the arrayed waveguides carefully and the cleaved facet should be polished further to be smooth and flat [48]. Dielectric or metal films (e.g., Cr-Au film) are usually needed to enhance the reflection efficiency [48–50], which makes the fabrication relatively complex. Furthermore, one should note that it is still difficult to achieve a high-quality reflector at the micrometric waveguide facet and consequently the performance of reflective AWGs is usually degraded [50, 51].

For SOI-nanowire AWGs, it becomes even more difficult to introduce conventional metal mirrors because of the small physical space. Alternatively, a pure-dielectric reflector based on photonic crystal (PhC) structures is a suitable option for realizing a reflective SOI-nanowire AWG as demonstrated in Figure 3A [27]. The PhC reflectors can be replaced by Bragg grating (i.e., a one-dimensional PhC structure) [30], or Teardrop reflector [52]. In this way, the fabrication of such an ultrasmall reflective AWG is compatible to the standard CMOS process and no additional fabrication process is needed in comparison with regular SOI-nanowire AWGs. Figure 3B shows the measured spectral responses for the eight channels of a 400 GHz-spacing reflective SOI-nanowire AWG with a footprint of 134 μm×115 μm. It can be seen that the excess loss of the fabricated reflective AWG (de)multiplexer is about 3~4 dB and the crosstalk is about -12 dB. As a comparison, we have also fabricated a 16-channel 200 GHz ultra-compact reflective SOI-nanowire AWG on the same chip, as shown in Figure 4A. The footprint is about 193 μm×168 μm, which is about twice larger than that of the 8-channel 400 GHz-spacing AWG. The measured spectral response is shown in Figure 4B. It can be seen that the channel crosstalk is high, which is mainly from the phase errors in the arrayed waveguides. This comparison indicates that a small footprint is indeed important for the device to achieve good performances.

As shown in Figures 3A and 4A, each arrayed waveguide of the reflective AWG has its own PhC reflector, which makes the layout design very flexible even when a very low or very high diffraction order is needed. It is also possible to use arrayed waveguides without any bends, which can minimize the length of the shortest arrayed waveguide. This is helpful to reduce the crosstalk resulting from the phase error in the waveguide array according to the theoretical analysis in Ref. [53].

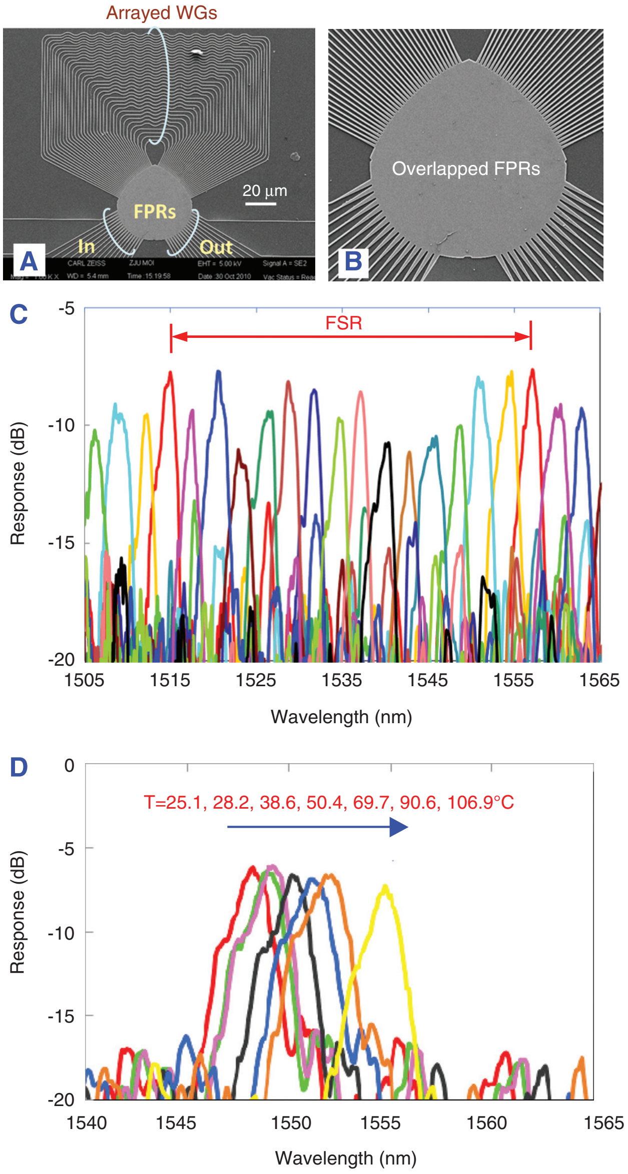

Figure 2 (A) SEM picture of a fabricated AWG router with microbends; (B) the enlarged view for the overlapped FPRs; (C) the measured spectral responses for the 15 channels; (D) the thermally-tunability of the spectral response.

2.1.2 Echelle diffraction grating (de)multiplexer

An EDG is another typical planar waveguide (de)multiplexer, which is very similar to a reflective-type AWG. An EDG has no arrayed waveguides but consists of a reflective grating [30], as shown in Figure 5. It is known that multimodal propagation in the FPR deteriorates insertion loss and channel crosstalk because multiple images are formed along the Rowland circle due to the mode dispersion [54]. Fortunately, the 220 nm-thick FPR only supports one guided-mode so that there is no performance deterioration caused by higher-order modes for an SOI-nanowire EDG [30].

A general issue for an EDG is that deeply etched grating facets with high verticality are usually required critically to minimize the excess loss [55]. Fortunately, when using a submicron (e.g., 0.22 µm)-thick SOI platform discussed here, the etching depth is small and the requirement for the sidewall verticality is relaxed. The reflection efficiency of the grating facets can be improved significantly by utilizing local Bragg mirrors at the facets [31]. For an EDG, the crosstalk is mainly from the facet position fluctuation in the reflection mirrors and the silicon thickness variation. The reported EDG usually has a crosstalk level around -20~-35 dB [30–33] and SOI-nanowire EDG (de)multiplexers have been used to realize a multi-channel communication link between two chips [4].

For an EDG the phase delay is obtained by a difference in path length between the grating teeth for a propagating beam in the FPR, which also work as the beam focusing region. This makes it potentially smaller than an AWG for the case with large channel spacing. On the other hand, an AWG can scale down to smaller channel spacing with less penalty than an EDG [26]. And the input/output waveguides of an EDG are sitting at the same side of the FPR, which makes an EDG not as flexible as an AWG. For example, an AWG can work in both directions for some applications [56] while an EDG cannot do so.

Table 1 shows the typical parameters for SOI-nanowire AWGs and EDGs reported in the past years. The devices used for photonic networks-on-chip are required to be ultrasmall due to the limited physical space and low loss is also desired according to the power budget of an optical interconnect link, which is different from conventional long-haul networks. Fortunately, low-loss SOI-nanowire AWGs and EDGs with ultrasmall footprints have been realized with optimized fabrication processes as well as improved designs in the past 10 years, as shown in Table 1. For example, the on-chip loss of an AWG/EDG can be lowered to around 2 dB by introducing some specific designs, e.g., bi-level taper structures for AWGs [26], Bragg-grating reflectors for EDGs [31]. Such loss reduction is helpful for realizing low power-consuming photonic networks-on-chip. The crosstalk of SOI-nanowire AWGs and EDGs has also been improved significantly as shown in Table 1. For an AWG, the crosstalk can be effectively reduced to about -20~-25 dB by minimizing the fluctuation due to the core-width variation through the way of enlarging core width in the straight regions [23–26]. In comparison with AWGs, EDGs are more fabrication tolerant since light is propagating in a slab where the thickness is usually controlled well in a small area and

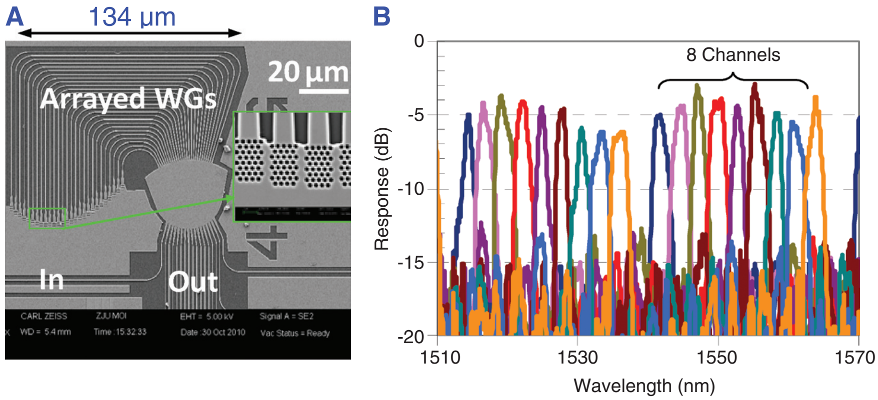

Figure 3 (A) An SEM picture of the fabricated reflective AWG (de)multiplexer with 8×400 GHz channels; inset: the enlarged view for PhC reflectors (the footprint 134 μm×115 μm); (B) the measured spectral responses.

consequently an SOI-nanowire EDG usually has lower crosstalk than an SOI-nanowire AWG (see Table 1). In Ref. [57], it has been demonstrated that error-free WDM transmission with four channels was achieved even when the crosstalk for the WDM filters is up to -17 dB. It is expected to realize error-free transmission with more WDM channels by using the improved SOI-nanowire AWGs and EDGs shown in Table 1.

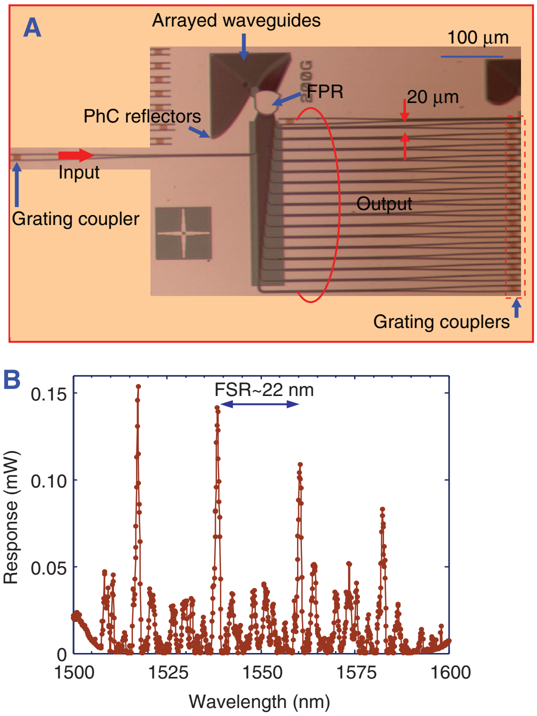

Figure 4 (A) An optical picture of the fabricated reflective AWG (de) multiplexer with 16×200 GHz channels (the footprint is about 193 μm×168 μm); (B) the measured spectral response for one channel.

2.2 Microring resonator (MRR) filters

An MRR usually has one or two couplers to be an all-passed filter or add-drop filter, as shown in Figure 6A-B, respectively. For a MRR, the important parameters include the resonance wavelength λ_{res}, the FSR, the 3 dB bandwidth $\Delta\lambda_{3dB}$, and the extinction ratio (ER) [35]. The bandwidth $\Delta\lambda_{3dB}$ and the ER are determined by the cavity loss and the coupling ratios of the couplers. When a small bandwidth $\Delta\lambda_{3dB}$ (i.e., a high Q factor) is desired, one need not only improve the fabrication processes to achieve a smooth waveguide with reduced scattering loss but also make the bending radius large enough to guarantee a small bending loss [58]. In order to have a high ER, the coupling ratio should be chosen appropriately according to the critical coupling condition [35]. As described in the introduction, a large wavelength window might be required for CWDM on-chip optical interconnects, and thus it will be interesting to have MRR filters with an ultra-large FSR and a large tunability range of wavelength, which is reviewed below.

2.2.1 Microring resonator (MRR) optical filters with an ultra-large FSR

The resonance wavelength of an MRR is given by the following equation: $\lambda_{res}=n_{eff}L_{cav}/m$, where n_{eff} is the effective index

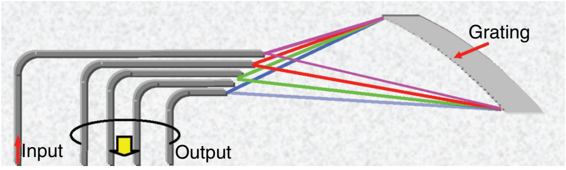

Figure 5 The structure of an EDG with four channels.

Table 1 Reported AWGs & EDGs on SOI nanowires.

Ref.	Year	Crosstalk (dB)	On-chip loss (dB)	Channel number× channel spacing	Waveguide size (nm²)	Footprint (μm×μm)	Area (mm²)
AWG [19]	2004	~-7	~8	8×3.2 nm	450×220	380×290	0.110
AWG [20]	2004	~-5	~10	17 x 6 nm	350×300	110×93	0.010
AWG [21]	2005	~-10	~1	9 x11 nm	350×300	60×70	0.004
AWG [23]	2005	-17~-20	2.2~5.2	16×1.6 nm	450×220	500×200	0.100
AWG [22]	2006	~-10	~10	5 x11 nm	500×250	40 x 50	0.002
AWG [24]	2006	-12	3.5	16×1.6 nm	450×220	425×155	0.066
AWG [25]	2010	<-18	~2.5	32×1.6 nm	500×300	370×500	0.185
AWG [26]	2010	~-25	1.1~2.4	8×3.2 nm	450×220	200×350	0.070
AWG [27]	2010	~-12	3~5	8×3.2 nm	500×220	115×134	0.015
AWG [29]	2011	-8~-10	~6	16×3.2 nm	500×220n	163 x147	0.024
EDG [30]	2007	~-30	~7.5	8×20 nm	500×220	280×150	0.042
EDG [31]	2008	~-25	~1.9	8×20 nm	500×220	280×150	0.042
EDG [32]	2009	16~-19	~ 3	8×3.2 nm	500×220	250×200	0.050
EDG [34]	2009	<-10	~10	21×1.0 nm	450×250	2000×1500	3.000
EDG [26]	2010	~-15	3~7	30×3.2 nm	450×220		0.500

of the eigenmode of the cavity waveguide, L_{cav} is the cavity length, m is the interference order. Accordingly one can achieve the equation for the FSR as follows: $FSR=\lambda_{res}/m'$, where $m'=m(n_g/n_{eff})$, the group index $n_g=n_{eff}-\lambda_{res}(\partial n_{eff}/\partial\lambda)$. It can be seen that the FSR is inversely proportional to the cavity length (i.e., the bending radius) [59–60]. Since the total bandwidth of a microring-based WDM system [61] is limited by the FSR of the MRR, a smaller MRR is desired to have a larger FSR so that more wavelength channels can be fitted to have higher aggregated data bandwidth [59]. For example, the ultra-large FSR is required to be more than 75 nm when a 48-channel WDM link with a channel spacing of 200 GHz.

For the case of using SOI nanowires, the bending radius can be as small as several microns [59, 60] so that the FSR is as large as several tens of nanometers, as shown in Figure 7A. For example, the FSR increases from 17 nm to 58 nm when the bending radius is reduced from R=5 μm to R=1.5 μm, as shown in Figure 7B and C. Therefore, a simple way to achieve ultra-large FSR is reducing the bending radius further, which can be realized by using e.g., suspended SOI nanowires with an improved index-contrast. Furthermore, when using MRRs as tunable optical filters, optical modulators, optical switches, etc, the size reduction is also helpful to reduce the power consumption, which is directly proportional to the circumference [59].

Another potential way to achieve a large FSR is to depress the resonance peaks except the one to be used so that there is only one major resonance peak with a high ER over a broad band, which indicates an ultra-large quasi-FSR. It is well known that a high ER is achieved for the resonance wavelengths when the following critical coupling condition is satisfied [62]

$$k^{(0)}_{2'1'}=k^{(0)}_{12}, \tag{7}$$

where the coupling ratios are defined as shown in Figure 6A. On the other words, when this critical coupling condition is broken, the resonance peak is depressed and the ER could be low. An MZI-coupled race-track resonator was proposed to modify the ER of one resonance wavelength by thermally tuning the coupling ratio of the MZI coupler [37, 63], which also enables to tune the 3 dB bandwidth [64]. By utilizing the wavelength-dependence of the MZI's coupling ratio, one can depress the resonance peaks except that one to be used so that there is only one major resonance peak over a broad band so that an ultra-large quasi-FSR is achieved as demonstrated in [65, 66].

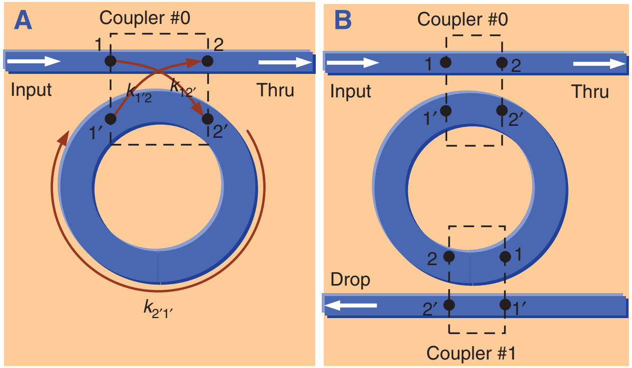

Figure 6 The schematic configurations of MRR devices: (A) an all-passed filter; and (B) an add-drop filter.

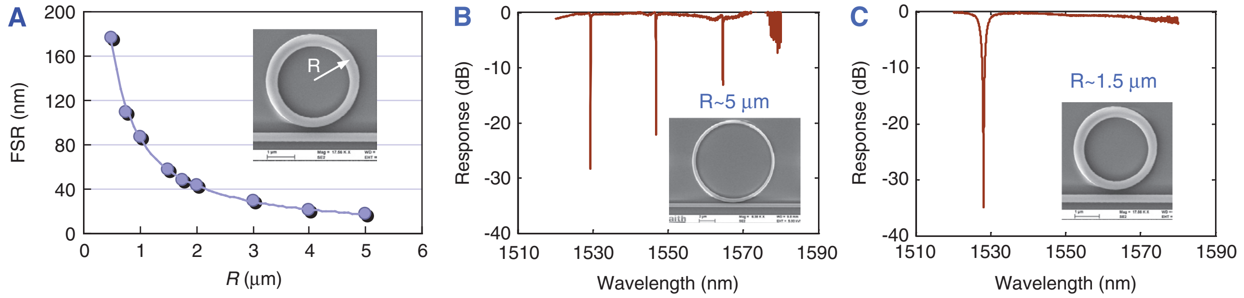

Figure 7 (A) The FSR as the bending radius decreases; the measured spectral response of the fabricated MRRs with (B) R=5 μm, and (C) R=1.5 μm.

As an example, Figure 8A shows the structure of a fabricated MZI-coupled MRR and the measured spectral response is shown in Figure 8B [66]. From this Figure, it can be seen that there is a major resonant wavelength λ_{MRR0} at around 1540 nm with a high ER (>25 dB) in the wavelength range from 1520 nm to 1630 nm (which is limited by the tunable range of the laser source used in the measurement). And the other resonant wavelengths in this range (1520–1630 nm) are depressed distinctly. It indicates that the MZI-coupled MRR has an ultra-large quasi-FSR (>120 nm). This can be also extended to the design of an MRR-based add-drop filter by combining a directional coupler (DC) and a MZI coupler.

As an alternative, MRR can also play the role as a wavelength-dependent coupler and thus one can build an add-drop filter with a MRR-based 2×2 coupler (coupler #0), as shown in Figure 9. These two rings have different bending radii (R_1 and R_2) so that their FSRs are different slightly and there is a common resonance wavelength around the desired wavelength (e.g., 1550 nm). Due to the Vernier effect, the period of the common resonance wavelengths will become very large. Here the MRR-based coupler (coupler #0) is design to have a high cross-coupling ratio $k^{(0)}_{12}$, at its resonance wavelengths (see Figure 10A) while another coupler (coupler #1) is a regular DC whose cross-coupling ratio $k^{(1)}_{12}$, is not strongly wavelength-dependent. In this way, the critical coupling to have a high ER occurs around the common resonance wavelengths. Otherwise, the critical coupling condition is broken and the resonance is depressed significantly, which gives an ultra-large quasi-FSR, as indicated by the calculated responses shown in Figure 10B and C. In this example, an SOI nanowire is used and the parameters are: R_1=5.56 μm (FSR_1≈16 nm), R_2=6.10 μm (FSR_2≈14.5 nm), the coupling ratio $k^{(0)}_{12}$,≈0.4, the coupling ratio between the input waveguide and ring #1 is about 0.4, the coupling ratio between the two rings is 0.08. From Figure 10B and C, it can be seen that an ultra-large FSR (>150 nm) is achieved.

2.2.2 MRR optical filters with large tunable range of wavelength

For an MRR, the resonance wavelength is usually tuned by introducing a refractive index change for the ring waveguide electrically or thermally [67–69], and the wavelength detuning $\Delta\lambda$ is given by $\Delta\lambda=(\Delta n_{\mathrm{eff}}/n_{\mathrm{g}})\lambda$. However, it is difficult to have a large wavelength detuning since the index change due to electrooptical (EO) or thermooptical (TO) effect is usually small. For example, when there is 100°C temperature increase for a SOI-nanowire-based MRR, the wavelength detuning is about $\Delta\lambda$≈8 nm only according to the TO coefficient (C_{TO}=1.8×10^{-4}/°C) of silicon. This tuning range of wavelength can be improved if a large change for the effective index is achievable. For example, a nano-slot waveguide proposed in [70] provides a potential way since its effective index n_{eff} changes very

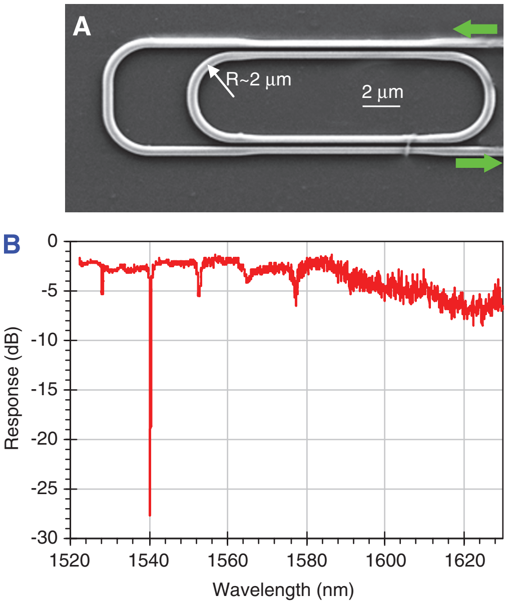

Figure 8 (A) The SEM image for a fabricated MZI-coupled MRR; (B) the measured transmission response of MZI-coupled MRR.

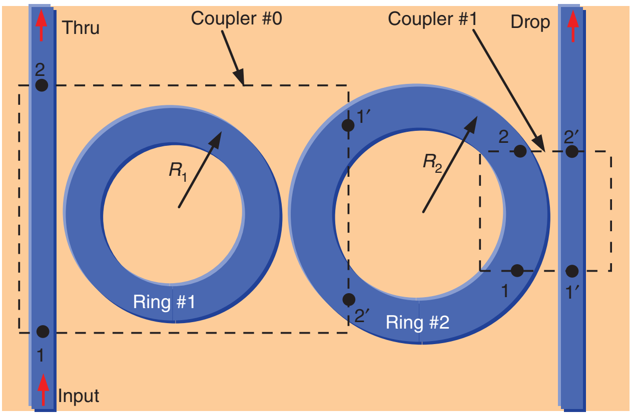

Figure 9 The schematic configuration of an MRR-coupled microring add-drop filter.

significantly as the nano-slot thickness changes due to the strong field enhancement in the nano-slot region. A suspended horizontal nano-slot waveguide (as shown by the inset in Figure 11) can be used so that the thickness of the nano-slot can be modified mechanically. Figure 11 shows the calculated effective index n_{eff} for such a suspended horizontal nano-slot waveguide as the nano-slot thickness h_{slot} varies from 5 nm to 60 nm. It can be seen that the change of the effective index n_{eff} is as large as 0.5 when the slot width changes from 5 nm to 30 nm mechanically. The corresponding wavelength tuning range is ultra-large (up to 200 nm) to cover a broad band. The mechanical tuning of a nano-slot can be realized by using e.g., optical forces [71], or electrostatic comb-drive actuators [72].

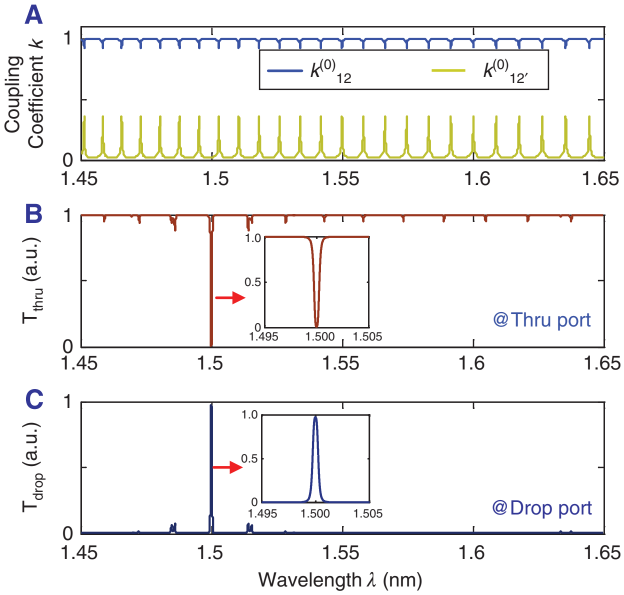

Figure 10 (A) The wavelength-dependent coupling coefficient $k^{(0)}_{12}$ and $k^{(0)}_{12'}$ of the MRR coupler (#0); (B) the response at the through port of the microring add-drop filter; (C) the response at the drop port of the microring add-drop filter. The insets show the responses around the resonance wavelength of 1500 nm.

When using regular SOI nanowires, a potential approach to achieve a large tuning wavelength-range is utilizing the so-called Vernier effect with a cascaded-ring system, which includes two cascaded rings (i.e., ring #1 and ring #2), as shown in Figure 12A and B [73–75]. These two rings have different FSRs (e.g., $\Delta\lambda_{\text{FSR1}}$=5.94 nm and $\Delta\lambda_{\text{FSR2}}$=5.70 nm) by choosing different radii (e.g., R_1=19.82 μm and R_2=20.62 μm). Figure 13A shows the calculated spectral responses of the drop ports for ring #1 and #2. When the *i*-th resonance wavelength $\lambda_{1(i)}$ of ring #1 is coincided with the *j*-th resonance wavelength $\lambda_{2(j)}$ of ring #2, there is a major peak (with an ER of >20 dB) locating at the common resonance wavelength $\lambda_{c(i)}$ as shown in Figure 13B. When ring #2 is tuned with a small resonance-wavelength shift $\Delta\lambda_2=(\Delta\lambda_{\text{FSR1}}-\Delta\lambda_{\text{FSR2}})$ by introducing an appropriate index change Δn_{eff}, the common resonance wavelength $\lambda_{c(i)}$ corresponding to the major peak has a shift as large as $\Delta\lambda=\Delta\lambda_{\text{FSR1}}$ (see the dashed curve in Figure 13B). It can be seen that the wavelength tuning efficiency E $(=\Delta\lambda/\Delta n_{\text{eff}})$ is multiplied by M times in comparison with a single-ring system $(E_2=\Delta\lambda_2/\Delta n_{\text{eff}})$, where $M=\Delta\lambda_{\text{FSR1}}/(\Delta\lambda_{\text{FSR1}}-\Delta\lambda_{\text{FSR2}})$. In this way, it is possible to achieve ultra-large tuning range with a small effective index change [74].

2.3 General issues for WDM filters based on SOI nanowires

2.3.1 The thermal issue

As presented in Section 2.1.2, the large TO coefficient (TOC) of silicon (dn/dT=1.8×10^{-4}/°C) makes these SOI-nanowire devices strongly temperature-dependent, which is good to realize efficient thermally-tunable WDM filters. On the other hand, however, a temperature controller has to be

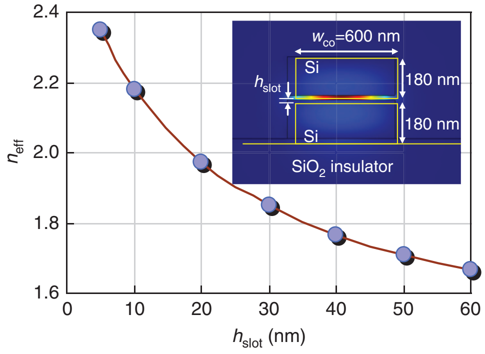

Figure 11 The effective index of a suspended Si nano-slot waveguide as the slot thickness varies.

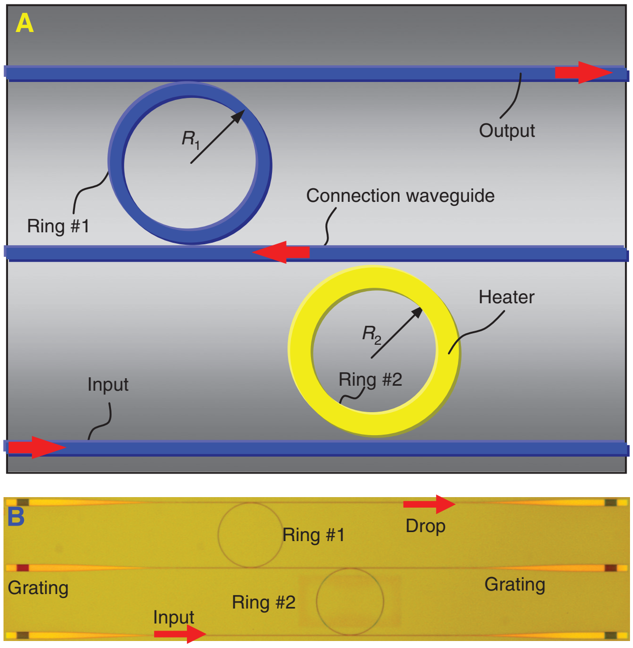

Figure 12 An MRR optical filter with a large tunable range of wavelength; (A) the top view; (B) the microscope picture.

employed to stabilize the chip temperature usually. In order to achieve athermal WDM filters (including AWGs and MRRs), a straightforward approach is introducing another material (like polymer) with negative TOC to compensate the positive TO effect of silicon, which is similar to those used in conventional optical waveguides [76–80]. One can fill the polymer material into the grooves in the silicon waveguide core region [81–83], which however requires very precise control for the waveguide fabrication. An alternative is using polymer as the upper-cladding of the waveguide [84–86]. In Ref. [84] a 1×8 SOI-nanowire AWG with a channel spacing of 400 GHz was realized experimentally. The wavelength temperature dependence of the AWGs is reduced to -1.5 pm/°C, which is much less than that of normal SOI AWGs. Another way to make temperature-insensitive WDM filters (e.g., AWGs, MZIs) is making arm waveguides consisting of two different sections (e.g., narrow and wide SOI nanowires), whose path-length differences are adjusted optimally [87–89]. In this way, one does not need to introduce any additional material (e.g., polymer) so that the fabrication is CMOS-compatible. The problem is that the diffraction order of the AWG is usually low, which limits its application in some degree.

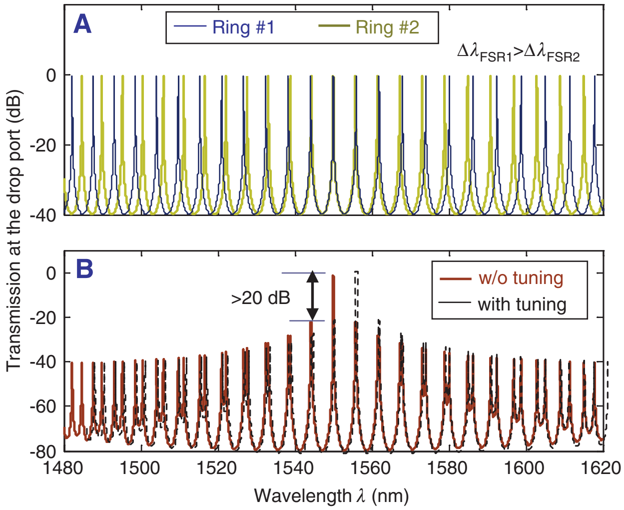

Figure 13 The calculated spectral responses for (A) ring #1 and ring #2; (B) the cascaded-ring system.

2.3.2 The polarization-sensitive issue

Due to the ultra-high index contrast and the submicron cross section, SOI nanowires usually have giant birefringence on the order of 10^{-1}, which makes SOI-nanowire PICs significantly polarization-sensitive [22]. For fiber-related applications, polarization-insensitive PICs are usually needed. Theoretically speaking, it is possible to make SOI nanowires non-birefringent by optimizing the waveguide dimensions, like those demonstrated for large SOI ridge waveguides [90–94]. However, it is very hard to achieve non-birefringent SOI nanowires experimentally because of the stringent fabrication tolerance. More importantly, the polarization dependent properties of SOI-nanowire devices are different from those devices based on micrometer optical waveguides. For example, for an SOI-nanowire AWG, not only the channel wavelength but also the channel spacing are polarization sensitive, which makes conventional polarization compensation approaches ineffective [95]. Some special approaches are proposed to minimize the polarization-sensitivity of SOI-nanowire photonic integrated devices including multimode interference (MMI) couplers, MRRs, and AWG (de)multiplexers [95–100]. A general solution to eliminate the polarization-sensitivity of silicon photonic integrated devices is using the so-called polarization-diversity technology [101–103]. In Ref. [103], a very smart design for a polarization diversity system was demonstrated to realize polarization-insensitive AWG by using a two-dimensional grating coupler, which simultaneously serves as a fiber-chip coupler, a polarization splitter as well as a rotator. However, it does not work for the case when the AWG needs to be integrated with other components in the same chip. In-plane polarization diversity devices will be needed for large-scale PICs. For example, in Ref. [56], an on-chip polarization diversity circuit is used to realize a polarization-diversified receiver chip by working together with a single Si$_3$N$_4$ AWG which has two signals running along opposite directions to ensure that the receiver is free of polarization-dependent wavelength shift. Polarization diversity technologies are not only essential for solving the polarization issues of SOI-nanowire PICs, but also the key for realizing the PDM technology. For such polarization diversity circuits, the polarizing beam splitter (PBS) and polarization rotator (PR) are the most important elements [101–103], which will be reviewed in the following section.

3 Polarization multiplexing and the devices (PBS, PR)

Polarization-multiplexing is attractive for photonic networks on-chip as a low-cost and simple way to improve the capacity, especially because planar optical waveguides have excellent polarization-maintaining ability and avoid the randomness of the polarization state of light. Figure 14 shows the schematic configuration of a PIC with the PDM technology. Here the PBS (or PBC) works as the (de)MUXer while the PR is utilized to generate two orthogonal polarization modes with the same light source to low the cost. High ER is desired for the PBS as well as the PR so that the channel crosstalk is low. Furthermore, it is also desired to achieve broadband PBSs and PRs, which make it possible to work together with the WDM technology to form a kind of hybrid multiplexing system. As classical elements, these polarization diversity components (including PBSs and PRs) are also very useful for many other applications, e.g., polarization transparent silicon nano-PICs [103], coherent optical communications [104], and integrated photonic quantum circuits [105]. Here we give a review for the recent work on ultrasmall broadband polarization diversity components on silicon.

3.1 Ultrasmall PBSs

It has been realized that most photonic integrated devices are polarization dependent due to the birefringence of optical waveguides (as summarized in Table 2), which provides various ways to realize waveguide-type PBSs, including multimode interferometers (MMIs) [106–110], DCs [111–118], MZIs [119–121], photonic crystal (PhC) structures [122–126], AWGs [127], MRRs [128], etc. Among them, a DC structure is an attractive option for PBSs because of its structural simplicity. Usually a symmetrical DC consisting of two identical coupling waveguides is used and the PBS length is chosen to be equal as p times of the coupling length L_{π_1} of one polarization and $(p+m)$ times of the coupling length L_{π_2} of the other polarization, in which way the PBS is long and narrowband intrinsically [112]. In contrast, asymmetrical coupling systems have been considered as an improved option to achieve ultra-short and ultra-broadband PBSs [102], for which the waveguides are optimized to satisfy the phase-matching condition for only one polarization so that complete cross-coupling occurs. On the other hand, the other polarization is likely to have significant phase mismatch due to the strong waveguide birefringence and consequently there is almost no cross-coupling, as shown in Figure 15A in principle. It can be seen that such a PBS is as short as the beat length for the cross-coupled polarization. According to the reciprocity of light, such a DC-based PBS can also be easily extended to be an add-drop device for the PDM system by introducing an add port, as shown in Figure 15B.

An asymmetrical coupling system can be constructed by including two or three non-identical waveguides with different propagation constants in the coupling region. An easy way to make two non-identical waveguides is simply choosing different widths (w_{co1}, w_{co2}) or heights (h_{co1}, h_{co2}) of the core, as shown in Figure 16. Regarding the fabrication processes of PICs, the option of modifying the core width only is preferred to avoid any additional etching process. However, for two straight optical waveguides with different core widths ($w_{co1} \neq w_{co2}$, $h_{co1}=h_{co2}$), their fundamental modes for any polarization have different effective indices and consequently the phase matching condition is not satisfied. Therefore, one cannot have efficient cross-coupling between their fundamental modes for any polarization.

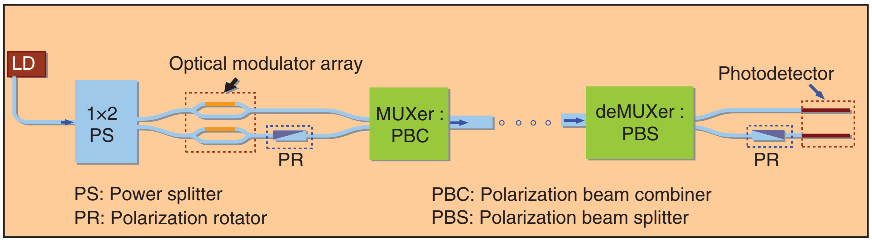

Figure 14 The schematic configuration of a PIC with the PDM technology.

Table 2 The polarization-dependence of several typical optical structures.

Structure	The device parameter which is polarization dependent
MMI [106–110]	The beat length L_π
MZI [119–121]	The central wavelengths
DC [111–118]	The coupling length/the coupling ratio
PhC/Grating [122–126]	The bandgap (reflection/transmission)
AWG [127]	The central wavelengths (@ $x=x_o$) The imaging position (@$\lambda=\lambda_0$)
MRR [128]	The resonance wavelength

Alternatively one can couple the fundamental mode in a narrow optical waveguide to the higher-order mode in a wide optical waveguide by optimally choosing their widths according to the phase matching condition (i.e., $n_{\text{eff0(I)}}=n_{\text{eff1(II)}}$). Another narrow optical waveguide can be placed at the other side of the wide waveguide as the output port, in which way the higher-order mode in the wide waveguide can be coupled to the fundamental mode of the output waveguide. Such a three-waveguide asymmetrical coupling system is achieved for realizing a PBS as shown in Figure 17A [129]. For example, when 220 nm-thick SOI nanowires are used, the optimal waveguide widths are w_1=410 nm and w_2=1.195 μm according to the phase matching condition for TM polarization, i.e., $n_{\text{eff0(I)\_TM}}=n_{\text{eff1(II)\_TM}}$. Figure 17B and C shows the simulated light propagation in the designed PBS when the TE_0 and TM_0 modes are launched at the input port, respectively. It can be seen that the TM_1 mode is excited in the middle wide waveguide and then coupled to the TM_0 mode in the narrow output waveguide. In contrast, there is no coupling for the input TE_0 mode due to the phase mismatching as expected. Figure 17D and E show the measured transmission spectral responses at the through port and the cross port when the TE- and TM-polarized light inputs, respectively. It can be seen that the TE-polarized light is output from the thru port and the TM-polarized light is output from the cross port. Some notable ripples are observed for TE polarization as shown in Figure 17E, which is partially due to the Fabry-Perot cavity effect resulting from the reflectivity of at waveguide facets. Another possible reason for the ripples of the transmission response at the cross port is the slight misalignment of input linearly polarized light [118]. Nevertheless, the present PBS has an ER of about 13dB over a large wavelength range, which can be improved further in the future.

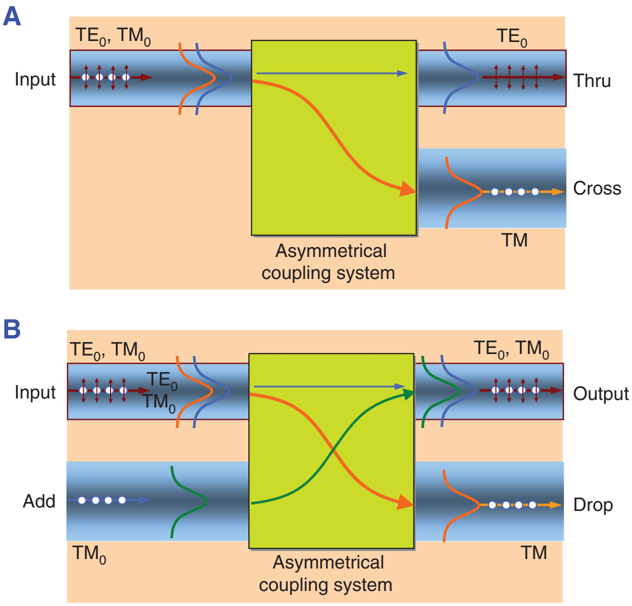

Figure 15 (A) The principle of a PBS with an improved coupling system; (B) an add-drop device for the PDM system.

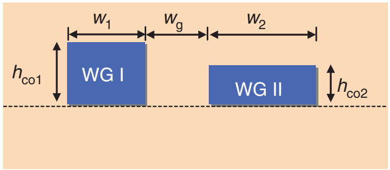

Figure 16 The cross section of the two waveguides for an asymmetrical coupling system.

An asymmetrical coupling system for the PBS can also be realized by using a bent asymmetrical directional coupler, as shown in Figure 18A. The phase matching condition for two parallel bent waveguides is given by $n_{\text{eff0(1)}}R_1=n_{\text{eff0(2)}}R_2$, where R_1 and R_2 are the bending radii of the narrow and wide optical waveguides. It can be seen that the phase matching condition can be satisfied by making the narrow optical waveguide have a larger bending radius than the wide optical waveguide (i.e., $R_1>R_2$) [130]. In Figure 18B and C, we show light propagation in the designed PBS with the following parameters: L_{dc}=4.5 μm, R_1=19.3 μm, R_2=20.0 μm, w_1=0.534 μm, w_2=0.46 μm, and w_g=203 nm. In this design, the phase matching condition is satisfied for TM polarization and the total length of the PBS is <10 μm. It can be seen that the TM_0 mode is cross-coupled very efficiently while the TE_0 mode is output from the through port without any coupling almost (see Figure 18B and C). Figure 18D and E show the simulated and measured transmission responses at the thru and cross ports of the fabricated PBS when TE and TM polarized lights are launched respectively. It can be seen that the simulation and measurement results agree well with each other. The ER for TE polarized light is more than 15 dB in a broad band. In contrast, for the TM polarization, the

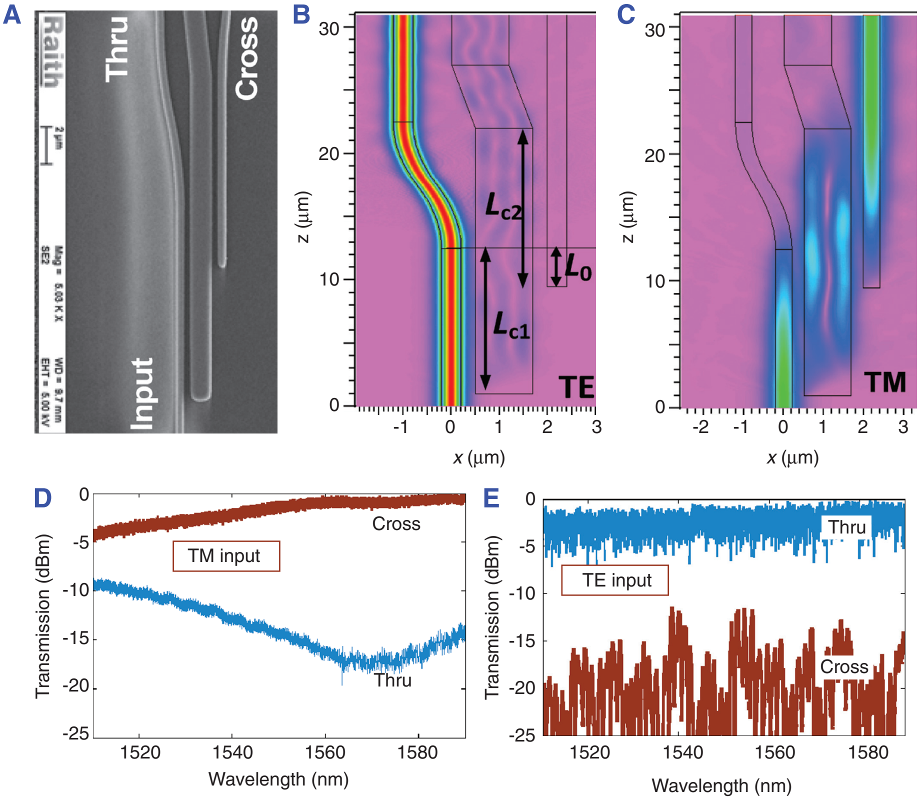

Figure 17 (A) The SEM picture for the fabricated PBS based on a three-waveguide asymmetrical coupling system; The simulated light propagation in the designed PBS: (B) TE; (C) TM; The parameters are h_{co}=220 nm, w_1=410 nm, w_2=1.195 μm, w_g=300 nm, L_{c1}=11.3 μm, L_{c2}=12.7 μm, and L_0= 3 μm; The measured spectral responses of the PBS at the thru/cross ports when the input light is with (D) TM and (E) TE.

response is wavelength-dependent because of the intrinsic wavelength-dependence of the evanescent coupling. It has also been shown that this PBS has large fabrication tolerance (e.g., Δw=±20 nm) [131].

Asymmetrical coupling systems can also be realized by introducing different types of optical waveguides with giant birefringence. For example, the regular SOI nanowire can be used as one of the coupling waveguides while the other waveguide in the coupling region can be made of some special optical waveguide, e.g., silicon nano-slot waveguides [132, 133], silicon hybrid plasmonic waveguides [134, 135], etc.

Figure 19A and B show the PBS based on an asymmetrical coupling system consisting of a nano-slot waveguide and a SOI-nanowire [132]. The S-bend section for the nano-slot waveguide plays a role as a mode converter between the input/output SOI-nanowire and the nano-slot waveguide (similar to that in Ref. [136]) so that the PBS becomes very compact (~7 μm) and also convenient to integrate with other SOI-nanowire components on the same chip. The transition loss and the back reflection at the junction of the mode converter are very small because the field amplitude at the nano-slot is negligibly small for the TM polarization that is coupled to the nano-slot waveguide [132]. In the coupling region, these two waveguides are designed to satisfy the phase-matching condition for TM polarization so that it is completely cross-coupled when choosing the length of the coupling region appropriately, as shown in Figure 19C. For TE polarization, it goes through the SOI-nanowire without coupling because of the phase mismatch, as shown in Figure 19D [132]. The present asymmetrical coupling system shown in Figure 19A has an add port so that it can also be used as an add-drop device for the PDM system.

A silicon hybrid plasmonic waveguide consisting of a SOI nanowire, a metal cap and an ultra-thin SiO_2 layer (h_d) between them (see Figure 20A [137]) can also be used to realize an asymmetrical coupling system for PBSs. For example, an ultrasmall (2×5.1 μm^2) PBS is presented by using a three-waveguides coupling system consisting of two SOI nanowires with a silicon hybrid plasmonic waveguide between them [134]. This asymmetrical coupling system was designed to make TM polarization cross-coupled and the total length of the designed PBSs (including the bending output section) is about 5~10 μm when the gap width is chosen as small as 100 nm. In Ref.

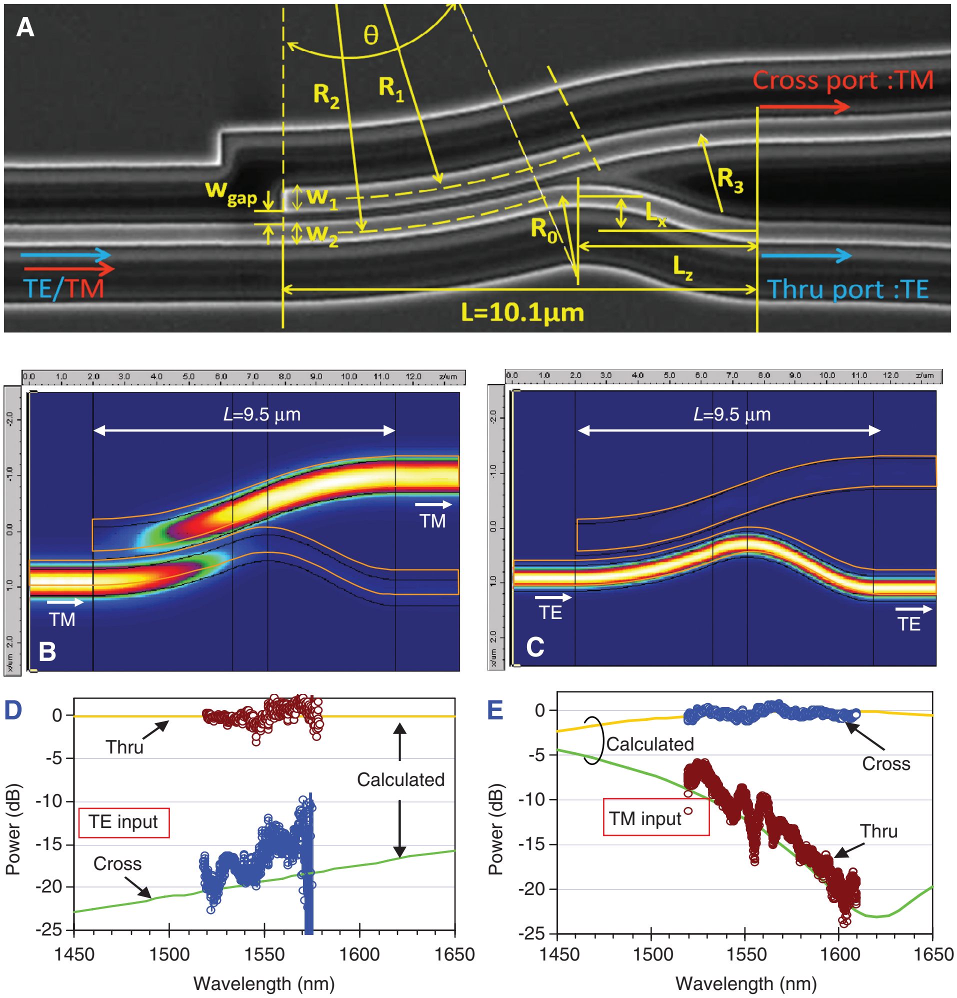

Figure 18 (A) The SEM picture for the fabricated ultra-short PBS based on a bent DC; The simulated light propagation in the designed PBS: (B) TM; (C) TE. The measured and stimulated transmission responses of the thru/cross ports for (D) TE polarization; (E) TM polarization; The parameters are L_{dc}=4.5 µm, R_1=19.3 µm, R_2=20.0 µm, w_1=0.534 µm, w_2=0.46 µm, and w_g=203 nm.

[138], we propose a simplified ultra-short PBS by using an improved asymmetrical coupler consisting of an SOI nanowire and a silicon hybrid plasmonic waveguide, as shown in Figure 20B. These two waveguides are designed optimally to make the phase-matching condition satisfied for TE polarization (instead of TM polarization). In this way, both two waveguides have relatively large widths around 300 nm and the length of the coupling region is only about 2.2 µm when the gap width is chosen as large as 200 nm, which makes the fabrication not difficult. A sharp bending is connected at the thru port to be as a compact polarizer by utilizing its large polarization dependent loss. The designed PBS (including the bending output section) has a footprint as small as only ~1.9×3.7 µm², which is the shortest PBS reported to date. Figure 20C show the simulated light propagation in the designed PBS with L_c=2.2 µm and R=1.3 µm when the TE_0 and TM_0 modes are launched. It has been shown that this PBS has a relatively high ER (~12 dB) over a ~120 nm bandwidth while the insertion loss is only 0.025 dB and 0.66 dB for TE and TM polarizations, respectively, which is mainly due to the metal absorption [138].

3.2 Polarization rotators

Great efforts have been made to realize polarization rotation by using the hybridized-mode interference or mode evolution in an asymmetrical structure, e.g., with bends, angled sidewalls, corner-cut cross sections, etc., as summarized in Table 3. In [139, 140], the structure with periodical sections of asymmetrical load is used to realize a PR which is quite long (~3 mm) and has a large excess loss due to the scattering as well as the mode-mismatching at the junctions between alternating sections. Similarly cascaded bent sections have also been used [141, 142] and

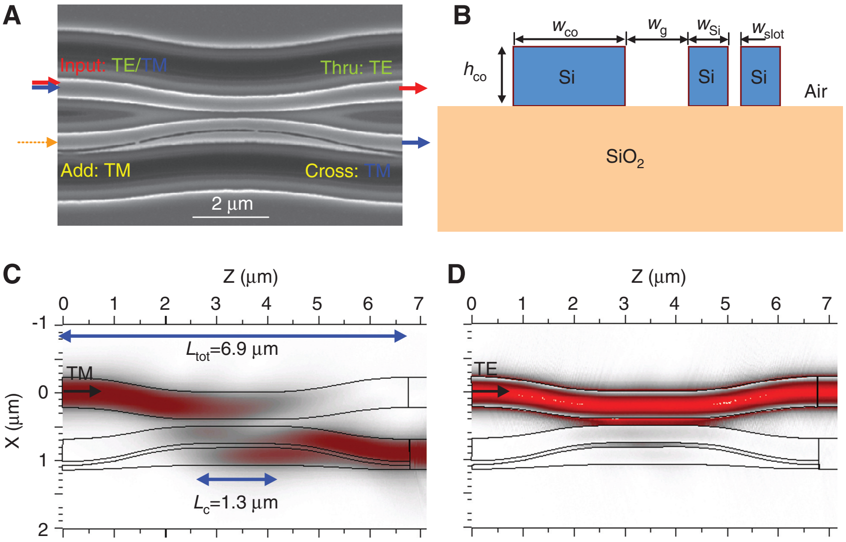

Figure 19 The PBS based on an asymmetrical coupling system consisting of a SOI-nanowire and a nano-slot waveguide: (A) the SEM picture; (B) the cross section. The simulated light propagation in the designed PBS with w_{co}=0.4 μm, w_{Si}=0.26 μm, h_{co}=250 nm, w_{slot}=60 nm, and w_g=100 nm: (C) TM; (D) TE.

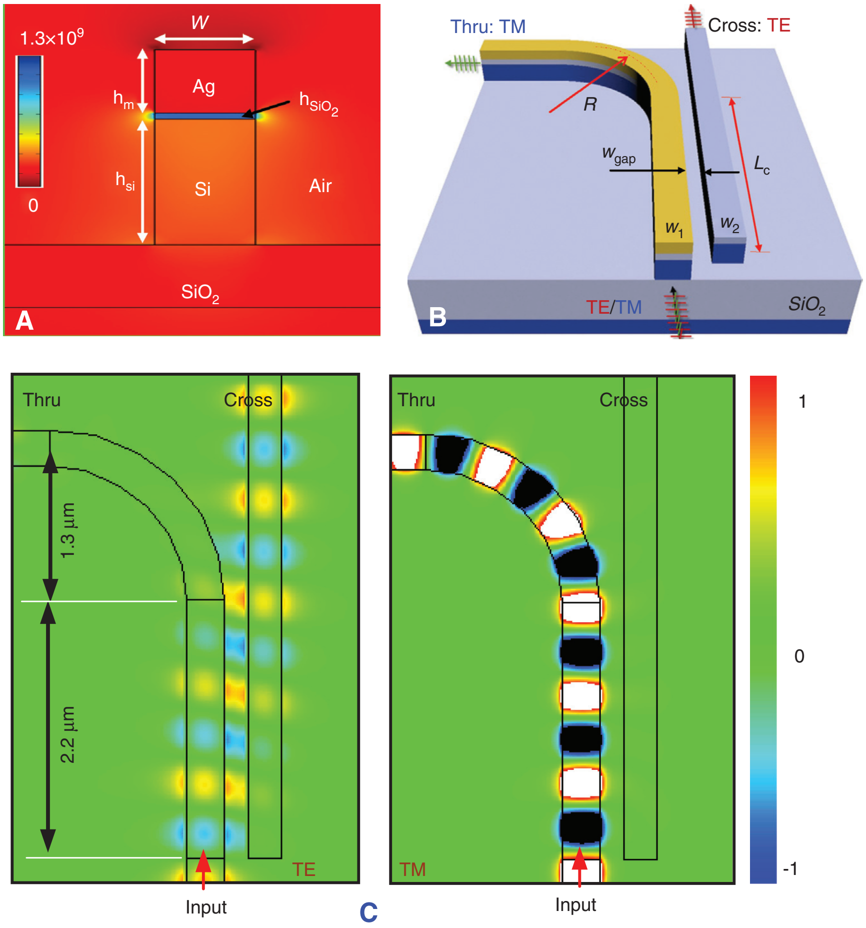

Figure 20 (A) The cross section of a silicon hybrid plasmonic waveguide with field enhancement in the low index region [137]; (B) the schematic configuration of the proposed PBS; (C) the 3D-FDTD simulation for the light propagation in the designed PBS when the input is TE or TM respectively.

the PR length is as short as ~60 μm with the assistance of slant waveguide sidewalls [141]. However, the design and fabrication are quite complex. Compact PRs (~150 μm) can also be realized by utilizing the reactive ion-etch lag effect [143], as well as angled InP waveguides [144]. For silicon photonics, PRs have been demonstrated by using micrometric SOI ridge waveguides with slanted sidewalls [145–148]. However they are as long as several hundred microns and the fabrication for slanted side-walls is not easy [148]. SOI-nanowire PRs have also been demonstrated with modified waveguide structures [149] and a 40 μm-long silicon PR based on mode evolution was demonstrated in Ref. [150], for which the fabrication is relatively easy because only a regular double-etching process is needed.

In [151], an ultra-short SOI-nanowire PR is proposed by introducing an input section, an output section and a polarization-rotation section with a cut corner (see Figure 21A and B). This polarization-rotation section supports two fully hybridized modes (see Figure 21C), which are excited equally almost and two-mode interference takes place along this section. The length of the polarization-rotation section is determined by the beat length $L_\pi=\pi/(\beta_0-\beta_1)$, where β_0 and β_1 are the propagation constants of these two hybridized modes, respectively. Figure 22A and B show the simulated light propagation in an optimized

Table 3 Summary of the reported PRs.

Ref	Structure	Features	Ref	Structure	Features
[139]	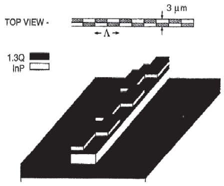	***Length***: 3700 μm ***ER***: ~10 dB ***EL***: 2~3 dB ***BW***: NA ***Fabrication***: Two-step etching	[143, 149]	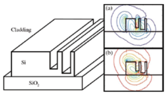	***Length***: 150 μm ***ER***: 14~16 dB ***EL***: ~0.7 dB ***BW***: 47 nm (for ER>9.5 dB) ***Fabrication***: RIE with lag effect
[140]	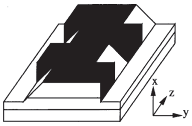	***Length***: ~900 μm ***ER***: ~18 dB ***EL***: ~0.25 dB ***BW***: NA ***Fabrication***: Special etching for asymmetric side-wall.	[150]	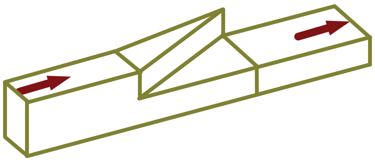	***Length***: <100 μm ***ER***: ~15 dB ***EL***: <1 dB ***BW***: >100 nm (for ER>13 dB) ***Fabrication***: Regular double etching
[141, 142]	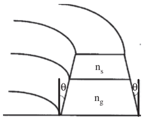	***Length***: ~60 μm ***ER***: ~20 dB ***EL***: 0.3 dB ***BW***: NA ***Fabrication***: Special etching for angled side-walls.	[151, 152]	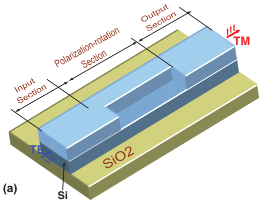	Length: 6~7μm ***ER***: >20 dB ***EL***: <0.1 dB ***BW***: >100 nm (for ER>15 dB) **Fabrication**: Regular double etching
[144]	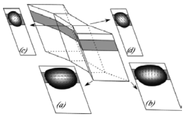	***Length***: ~50 μm ***ER***: ~20 dB ***EL***: ~1 dB ***BW***: 100 nm (for ER>15 dB) ***Fabrication***: Special etching for angled side-wall	[153]	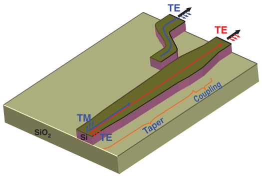	***Length***: <100 μm ***ER***: ~17 dB ***EL***: <0.1 dB ***BW***: >100 nm (for ER>10dB) ***Fabrication***: Single-step etching
[145–148]	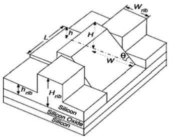	***Length***: 10^2~10^3 μm ***ER***: >20 dB ***EL***: ~0.2 dB ***BW***: 100 nm (for ER>20 dB) ***Fabrication***: Special etching for angled side-wall	[154]	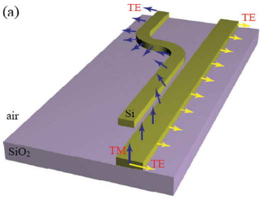	***Length***: <100 μm ***ER***: ~12 dB ***EL***: ~0.6 dB ***BW***: 35 nm (for ER>12 dB) ***Fabrication***: Single-step etching

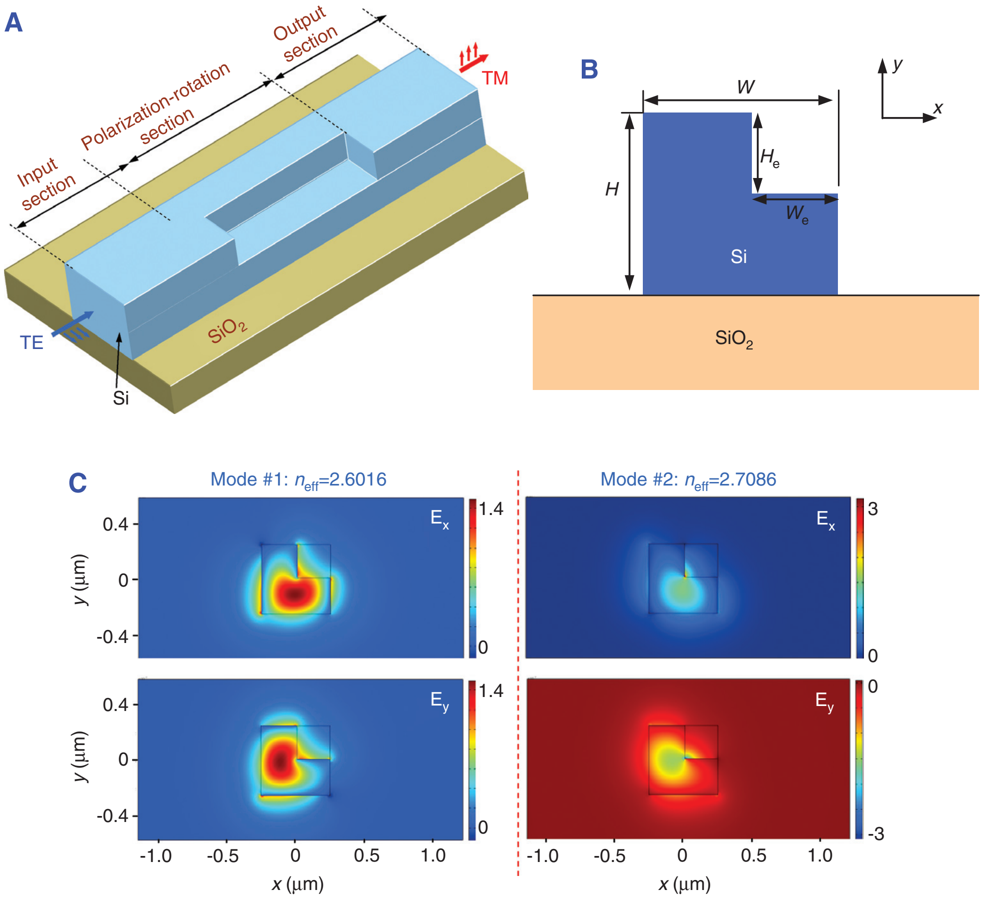

Figure 21 (A) The schematic configuration of the present PR; (B) the cross section of the asymmetrical SOI nanowire; (C) the field distributions of the two hybridized modes.

PR with the following parameters: H=500 nm, W=500 nm, W_e=240 nm, and H_e=240 nm [151]. It can be seen that the input TE polarization mode is successfully converted to the TM polarization mode at the output within a very short lengths (L_c≈7μm), which is much shorter than those previously reported. Recently a slightly modified PR based on SOI nanowires was demonstrated experimentally [152] to show that the TE-TM polarization rotation efficiency is as high as -0.51 dB over a wavelength range of 80 nm.

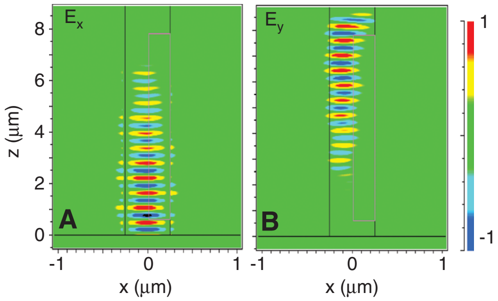

Figure 22 The simulated light propagation in the designed PR when it is with TE input: (A) E_x and (B) E_y. Here W_e= H_e=240 nm [151].

In Ref. [153, 154], novel designs with a simple fabrication (needing one-step etching only) are proposed and demonstrated to enable polarization splitting and rotation simultaneously, which is very attractive for ultracompact polarization diversity circuits. In Ref. [153], the proposed polarization splitter-rotator (PSR) consists of a taper and an asymmetrical directional coupler, as shown in Figure 23. The taper section is designed to realize the conversion from the TM_0 mode to the higher-order TE mode by utilizing the mode hybridization and coupling in a high index-contrast optical waveguide with an asymmetrical cross section. For example, when the upper-cladding index of an SOI nanowire with h_{co}=220 nm is not equal to that of the under-cladding layer (SiO_2), there exists mode-hybridization in the region around w_{co}=0.76 μm, as shown in Figure 24A. Figure 24B and C show the electrical-field profiles (E_x and E_y) of the two hybridized modes when w_{co}=0.76 μm. It can be seen that the x- and y-components of the electrical fields are comparable.

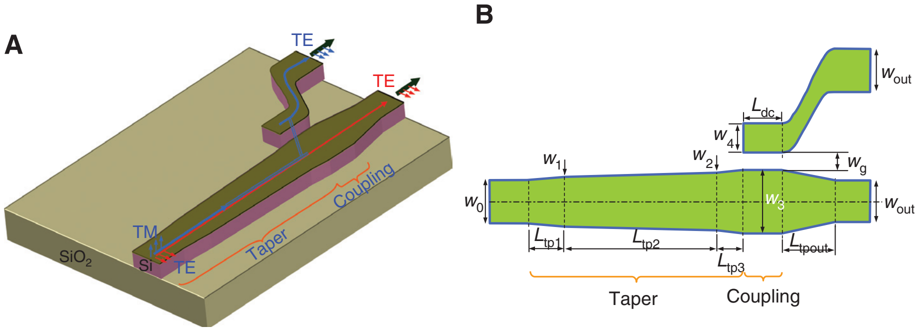

Figure 23 The structure of the PSR consisting of an adiabatic taper and an ADC [153], (A) a 3D view; (B) a top view.

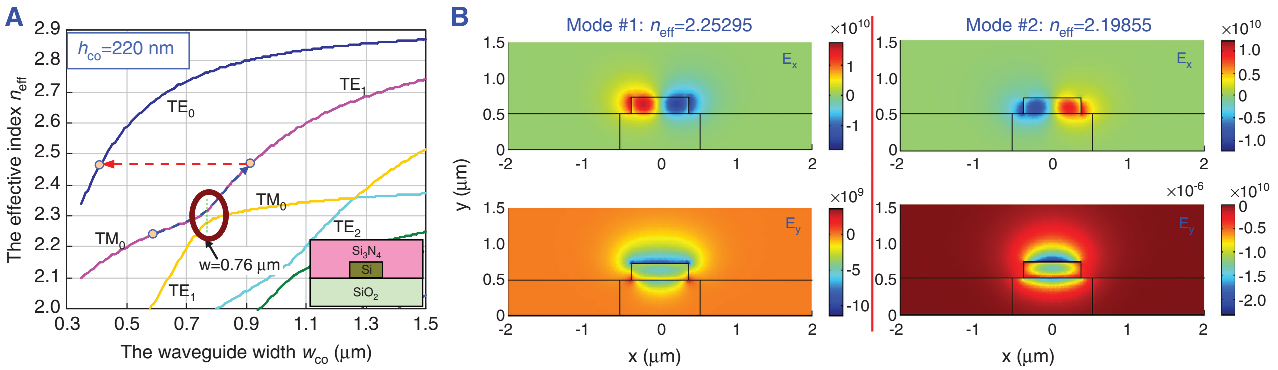

Figure 24 (A) The effective indices for the eigen-modes of SOI nanowires with Si_3N_4 cladding (n=2.0). Here the Si thickness h_{co}=220 nm; (B) The field profiles for the hybridized modes for the SOI nanowire with w_{co}=760 nm, h_{co}=220 nm, and n_{SiN}=2 (the upper-cladding).

Due to this kind of mode hybridization, a mode conversion will happen between the TM_0 mode and the TE_1 mode when light propagates along a width-varying taper section [153–155], as shown in Figure 25A. This TE_1 mode is then coupled to the TE_0 mode of an adjacent narrow waveguide by using an asymmetrical DC (ADC) cascaded at the end of the taper as shown in Figure 23A. As a result, the launched TM_0 mode at the input end is converted into the TE_0 mode at the cross port finally (see Figure 25A). In contrast, the input TE polarization keeps the same polarization state when going through the adiabatic taper structure and is not coupled to the adjacent narrow waveguide due to the phase mismatching, as shown in Figure 25B. Such a PSR has a bandwidth of over 70 nm and the tolerance for the width deviation is about $-10\text{ nm}<\Delta w<20\text{ nm}$ for an ER of >10 dB. A larger bandwidth and fabrication tolerance can be achieved by choosing a longer taper [153]. Such mode conversion from the TM_0 mode to the higher-order TE mode was also observed theoretically and experimentally in submicron SOI ridge optical waveguide tapers [156]. For submicron SOI ridge optical waveguide, which is usually asymmetrical in the vertical direction even with a

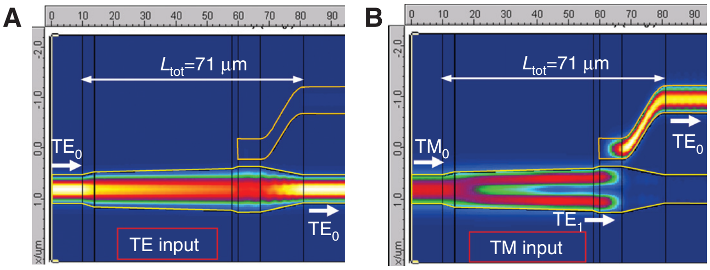

Figure 25 The simulated light propagation in the designed PSR when the input field is TM polarization (A), and TE polarization (B). Here the taper lengths are: L_{tp1}=4 μm, L_{tp2}=44 μm, and $L_{tp3}=L_{tp1}(w_3-w_2)/(w_1-w_0)$. The other parameters are w_0=0.54 μm, w_1=0.69 μm, w_2=0.83 μm, w_3=0.9 μm, w_g=0.15 μm, and L_{dc}=7.0 μm.

SiO_2 cladding, one can achieve mode conversion conveniently by utilizing an adiabatic taper. This paves a way to make polarization handling devices based on submicron SOI ridge optical waveguides.

4 Spatial division multiplexing (SDM) Devices: multi-core and multimode

For SDM technology, multiple channels of signals are carried by different cores or modes in parallel, which is important for long-haul optical fiber communications to higher capacity [7, 8]. SDM is also of interest for optical interconnects in data centers where upgrading an existing network or installing a new network is relatively simple [157–160]. It is even more convenient to apply SDM to the photonic network on-chip because the optical signal propagates along planar optical waveguides within the chip and the eigen-modes could be converted, transferred, as well as coupled conveniently between planar optical waveguides with some specific structures.

For the approach of using the multi-core SDM technology for photonic networks on-chip, the advantage is that the device design are easily because one does not need to deal with multiple modes. However, the drawback is the footprint issue and the increased circuit complexity. On the other hand, when using the multimode SDM technology, the waveguide design should be avoid any undesired mode coupling/conversion to low the channel crosstalk. For example, a multimode waveguide cannot be bent sharply and one has to introduce a large bending radius [161]. Besides, it is not easy to handle too many modes (e.g., >10) in a planar waveguides due to the mode coupling and crosstalk. Therefore, a potential way is combining the multi-core and multi-mode approaches to be a two-dimensional SDM technology for achieving many channels when needed. In the following section, we review the recent results for (de)MUXer devices useful for SDM technology.

Several kinds of structures for mode-(de)MUXer have been proposed. In Ref. [162, 163], a design based on multi-mode interference is proposed, which however works for two channels only and not easy to extend for more channels. Adiabatic mode-evolution couplers have been also proposed to realizing the multiplexing of only two modes [162, 163]. However, these devices suffer from several drawbacks, e.g., large footprints (~90 μm long for 2-channel multiplexing [162]), or reliance upon complicated waveguide cross-sections.

In Ref. [10, 164], a 1×N (N≥4) mode-(de)MUXer consisting of cascaded ADCs based on thin SOI nanowires (e.g., h=220 nm) was proposed as shown in Figure 26. The i-th ADC is formed by putting a narrow access waveguide close to the wide bus waveguide to form an evanescent coupling region. The bus waveguide consists of N straight segments whose widths are different and an adiabatic taper is inserted between the adjacent two straight segments. The width w_i of the i-th straight segment is optimized according to the phase matching condition so that the fundamental mode of the narrow access waveguide can be coupled to the i-th higher-order mode in the bus waveguide completely. On the other hand, those undesired eigen-modes will not be excited almost due to the significant phase mismatching and consequently the crosstalk between channels is low in principle.

As an example, a 1×4 mode (de)MUXer is designed for TM-polarization operation. When the narrow access waveguides are designed to have the same width w_a=0.4 μm, the optimal widths for straight sections of the bus waveguide are chosen as: w_1=1.02 μm, w_2=1.68 μm, and w_3=2.35 μm according to the phase matching conditions for the first, second and third higher-order modes, respectively. With a 3D finite-different time-domain (3D-FDTD) simulation, the optimal lengths for the coupling regions are achieved as L_{c1}=4.5 μm, L_{c2}=7.0 μm, and L_{c3}=9.7 μm when the gap width w_g=0.3 μm (see variables labeled in Figure 26). Figure 27A–C shows the simulated light propagation in the designed ADCs. It can be seen that light is efficiently coupled from the TM_0 mode in the narrow access-waveguide to the desired higher-order mode in the wide bus-waveguide and very little power is left in the access

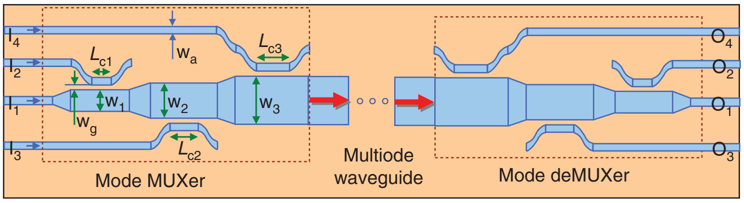

Figure 26 Schematic configuration of the proposed mode MUXers and deMUXers with 4 channels.

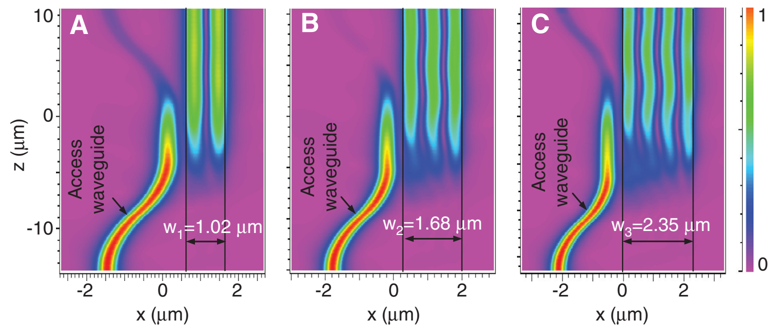

Figure 27 The simulated light propagation in the designed *i*-th stage ADC, (A) *i*=1; (B) *i*=2; (C). *i*=3.

waveguide. The theoretical excess loss of the designed ADCs is almost zero (<0.1 dB) and the channel crosstalk at the central wavelength is also very low (<25 dB).

Figure 28 shows the SEM picture for the fabricated chip, which includes a 4×1 mode MUXer, a 1×4 mode deMUXer, and a multimode straight waveguide between them (refer to Figure 26). Figure 29A–D show the measured transmission responses at all output ports O_1, O_2, O_3, and O_4 when light is input from port I_1, I_2, I_3, and I_4 respectively. From these Figures, it can be seen that light outputs from the corresponding output port as designed. For example, when light is input from port I_1 of the MUXer, the output power from the port O_1 of the deMUXer is the maximum. The total insertion loss is about 12~13 dB, which is mainly from the large fiber-coupling loss, since there is no mode-converters at the input/output ends of the chip. By comparing to the transmission response for straight waveguides in the same chip, the (de)MUXer shows low excess loss (<0.5 dB), which is consistent with the theoretical analysis. From Figure 29A–D, it can be seen that the crosstalk is lower than 20 dB in a broad wavelength-band, which makes it possible to work together with WDM for forming a kind of hybrid multiplexing technology when the capacity is desired to be improved further. In Ref. [165], a microring-based hybrid multiplexer was demonstrated to achieve simultaneous mode and wavelength division multiplexing on chip. Error free transmission ($BER<10^{-12}$) was realized by using a microring multiplexer with a crosstalk of about -13dB. Therefore, the present low-loss and low-crosstalk mode (de)MUXer should be very useful for the future applications.

For an optical interconnect link with multimode SDM technology, the multimode bus waveguide might be bent in order to change the light propagation direction to the distinction. Here we give a short discussion on light propagation in a 90°multimode bending waveguide (BWG) connecting to a straight waveguide (SWG). It is well known that a singlemode SOI nanowire can enable an ultra-sharp bending (~μm) with a low loss (including the pure bending loss and the transition loss) [44]. However, for a sharply bent multimode SOI nanowire, the modal field peak will shift outward notably. Consequently, when light propagates along an SWG connected to a BWG with a bending radius *R*, large transition loss and mode crosstalk are introduced due to the mode mismatch if the bending radius *R* is small. Figure 30A–D show the mode conversion efficiencies from the input modal field in the SWG to the eigenmodes in the BWG when the input field is the TM_0, TM_1, TM_2, and TM_3 mode of the SWG, respectively. From this Figure, it can be seen that the desired mode coupling efficiency (from TM_{i_SWG} to TM_{i_BWG}) decreases as the bending radius decreases, which is due to the increased mode mismatching. On the other hand, the undesired mode coupling (from TM_{i_SWG} to TM_{j_BWG}, $j\neq i$) increases as the radius *R* becomes smaller. For example, when choosing *R*=240 μm, the mode coupling ratio is very small (e.g., ~0.001 or smaller) from TM_{i_SWG} to TM_{j_BWG} ($j\neq i$). Figure 31A–D show the simulated light propagation in the structure consisting of a SWG and

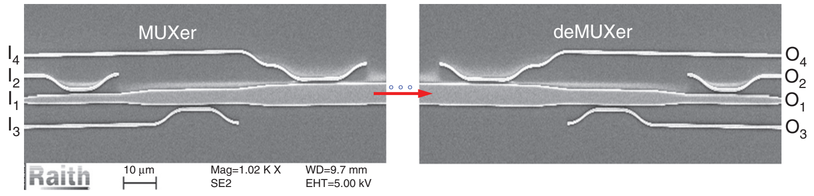

Figure 28 SEM picture for the 4×1 mode MUXer and 1×4 mode deMUXer integrated on the same chip.

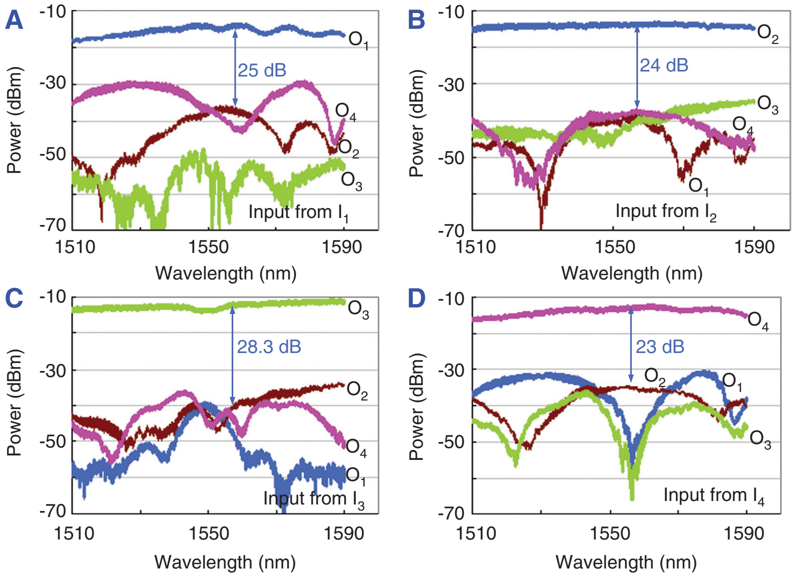

Figure 29 The measured responses at output ports (O_1, O_2, O_3, and O_4) when light is input from port: (A) I_1; (B) I_2; (A) I_3; (B) I_4.

a BWG with R=240 µm when the input is the TM_0, TM_1, TM_2, and TM_3 modal fields, respectively. It can be seen that there is multimode interference effects, which indicates that more than one modes are excited as predicted. Therefore, the bending radius has to be large to depress the undesired mode coupling / crosstalk.

In order to achieve a small bending radius as well as low mode crosstalk, one can reduce the mode mismatching by modifying the refractive index profile with the assistance of transformation optics theory [161]. Another simple way is introducing a bending section with a gradually-varying curvature, which has been applied to bent singlemode SOI nanowires successfully [166]. When the bending radius changes adiabatically, both transition loss and mode coupling can be depressed significantly. For example, we design modified bending multimode sections for the bus waveguide, as shown in Figure 32A–D, in which there are several sub-sections whose bending radii

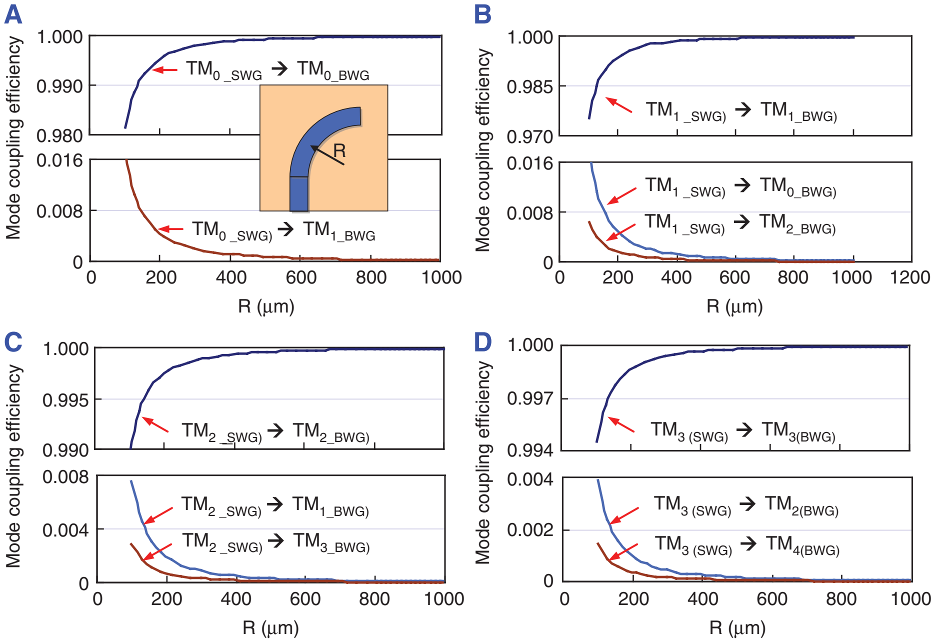

Figure 30 The mode conversion efficiency when light is launched from a straight waveguide (SWG) to a bent waveguide (BWG) with a bending radius *R*. The input fields are the TM_0 (A), TM_1 (B), TM_2 (C), and TM_3 (D) modal fields of the straight waveguide respectively.

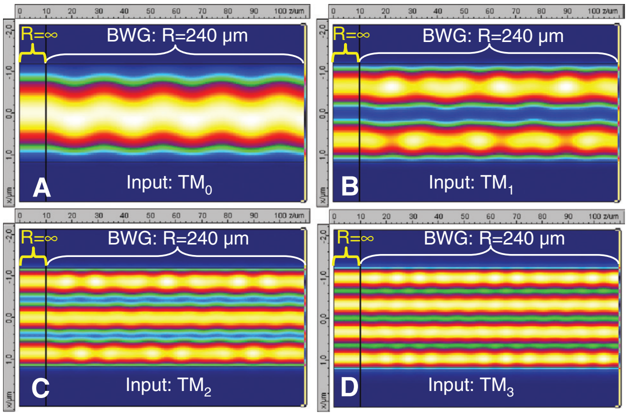

Figure 31 Light propagation in the designed 90°-bending when the input field is the (A) TM_0, (B) TM_1, (C) TM_2, and (D) TM_3 modes of the SWG, respectively.

are chosen as R=∞, 400, 200, 130, 100, 78, 62 µm. Each sub-section (except that one with R=62 µm) is 3.5 µm long. Figure 32A–D show light propagation in the designed 90° bent section when the input field is the TM_0, TM_1, TM_2, and TM_3 modes, respectively. From the comparison between Figure 31A–D and Figure 32A–D, it can be seen that the mode coupling becomes smaller and the crosstalk is reduced with the modified 90° bent section.

Another potential way to overcome the multimode bending issue is introducing a tall and narrow multimode bus waveguide for the ADC, whose cross section is shown in Figure 33. The multimode waveguide supports multiple higher-order modes in the vertical direction while it is quasi-singlemode in the lateral direction. In this way, the bending radius could be as small as several microns while the etching process becomes a little more complicated in comparison with that shown in Figure 26 because double-etching process is needed and the etching depth should be controlled very well. Furthermore, the etching process should be well optimized to have vertical and smooth sidewalls regarding to the high aspect ratio.

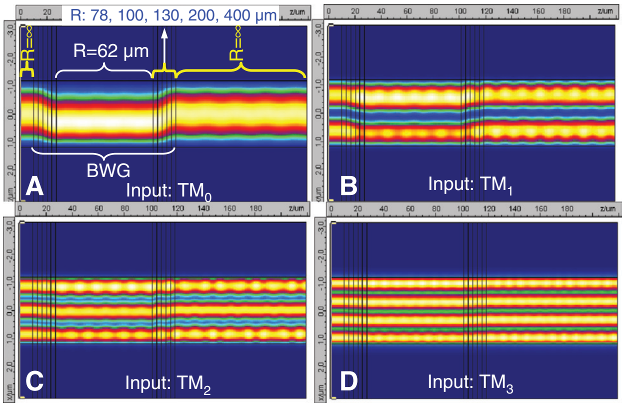

Figure 32 Light propagation in the modified 90° bent section when the input field is the (A) TM_0, (B) TM_1, (C) TM_2, and (D) TM_3 modes of the SWG, respectively.

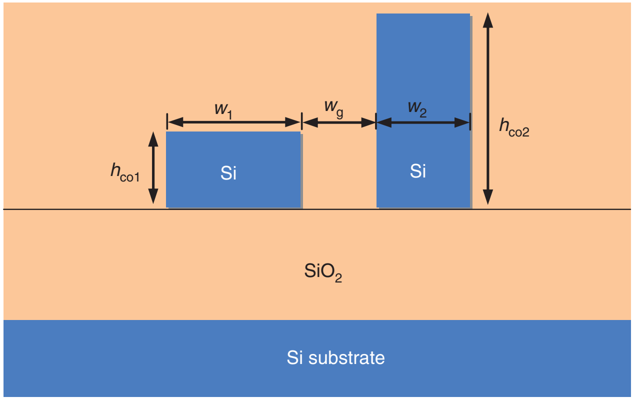

Figure 33 The cross section of an ADC consisting of a singlemode waveguide and a narrow multimode bus waveguide.

5 Outlook

5.1 Hybrid multiplexing technology

Table 4 shows the typical channel number for the multiplexing technologies discussed above. When using any one of the multiplexing technologies alone, the channel number is usually around 10 in practice currently and the link capacity is not more than 1Tbps by assuming that the bit rate is up to 100 Gbps. Therefore, the exponentially increasing demands for high link capacity (e.g., 10 Tbps) cannot be satisfied in the future. One solution is combining several multiplexing technologies to realize a multi-dimensional hybrid multiplexing technology. For example, one can use the PDM and multimode SDM technology to achieve more than 10 channels to support ~1 Tbps capacity with single-wavelength light carrier. WDM technology is then used together to enhance the link capacity of a single waveguide to about 100 Tbps with tens of channels. The optical-interconnect capacity can be further improved with the multi-core waveguide by introducing multi-core SDM technology. With this kind of

Table 4 Summary for the multiplexing technologies.

	WDM	PDM	Multimode SDM	Multi-core SMD
Channel number	4~100	2	2~8	1~10

multi-dimensional hybrid multiplexing technology, it is possible to achieve a capacity up to 1Petabit/s.

In order to realize the multi-dimensional hybrid multiplexing technology, the key is the hybrid (de)multiplexer for the transmitter and the receiver, which includes different types of multiplexer devices on a single chip. In this case, the related multiplexers should be designed to be compatible with each other. Figure 34 shows an example of using the PDM and multimode SDM technology to achieve ~1Terabit/s capacity with a single wavelength carrier. Here the mode MUXer should be designed to combine the eigenmodes for both polarizations. Alternatively, this can be also realized by cascading mode MUXers and a PBS with the ability to deal with higher-order modes for both polarizations, which is however a challenge because almost all the conventional PBSs are working for the fundamental modes of TE and TM polarizations. In order combine the WDM and PDM/SDM technologies, a simple way is putting WDM filters before the mode MUXer, for which the polarization-handling devices as well as the mode MUXers should be with a broad band. However, lots of waveguide crossings will be introduced for the chip layout, which causes some excess losses. The other option is putting mode MUXers before a WDM filter. In this way the WDM filter is required to have the same central wavelength for the fundamental and higher-order modes (which is a big challenge). Therefore, it can be seen that some novel devices are desired to realizing the multiplexing technologies for future on-chip optical interconnects.

5.2 Bidirectional multiplexing technology

In order to establish the communication between two chips, one should setup bidirectional optical interconnects, which usually are realized by choosing different carrier wavelengths for the forward and backward directions [167–170]. Bidirectional transmission usually has suffered from its sensitivity to backreflections, which lead to crosstalk between opposing transmitted channels and oscillation in bidirectional amplifiers. In order to solve this issue, a three-port bidirectional isolator was demonstrated [171]. Recently an integrated bidirectional optical amplifier (BOA) is proposed to allow amplified bidirectional communication of an entire WDM comb on a single link without crosstalk- and back-reflections-induced penalties, as shown in Figure 35 [172], where the four rings in the circuit have a non-reciprocal behavior [173]. For example, λ_1 and λ_3 are the CCW wavelength resonances of the rings 2 and 4, while λ_2 and λ_4 are the CW wavelength resonances of the rings 1 and 3. The two channels with λ_1 and λ_3 are injected from Port 1 and dropped to the amplifier through ring 2, and finally exit from Port 2 through the ring 4. In contrast, the back-reflections from the amplifier are not coupled back to the Port 1 and propagate towards Port S2. The reason is that ring 1 and ring 2 are out of resonance at λ_1 and λ_3 due to the non-reciprocal effect. Furthermore, the back reflections from Port 2 at λ_1 and λ_3 propagate back to Port S4 because both ring 4 and ring 3 are out of resonance in the CW direction at λ_1 and λ_3. The light injected from port 2 has similar behavior of propagation. In this way, it allows simultaneous amplification of counter-propagating WDM interleaved grids with a single amplifier (e.g., hybrid III-V semiconductor optical amplifiers).

When it is desired to used the same wavelength for a bidirectional link to avoid any additional cost for modifying the lasers, a potential simple way is using two orthogonal polarization states for the bi-directional link by utilizing the polarization handling devices (including PBSs and PRs) discussed in Section 3. Another potential way is introducing non-reciprocal devices, e.g., circulators. In Ref. [173], four-port integrated optical circulators based on MRRs have been presented, as shown in Figure 36A and B. A thin YIG (yttrium iron garnet) layer is deposited on the top of the SiN ring waveguide to achieve the magnetic-optical effect for non-reciprocity. By

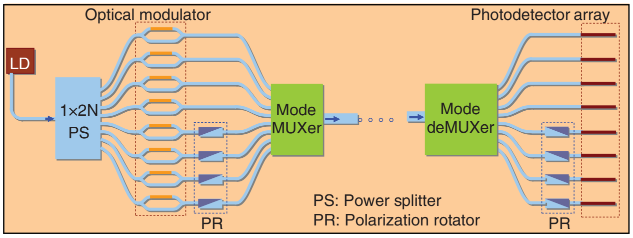

Figure 34 The schematic configuration of a hybrid multiplexed optical interconnect link combining the multimode SDM and the PDM technologies.

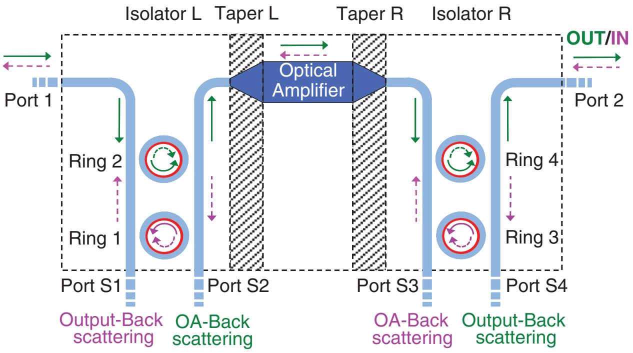

Figure 35 Bidirectional optical amplifier (BOA) layout with non-reciprocal ring resonators [172].

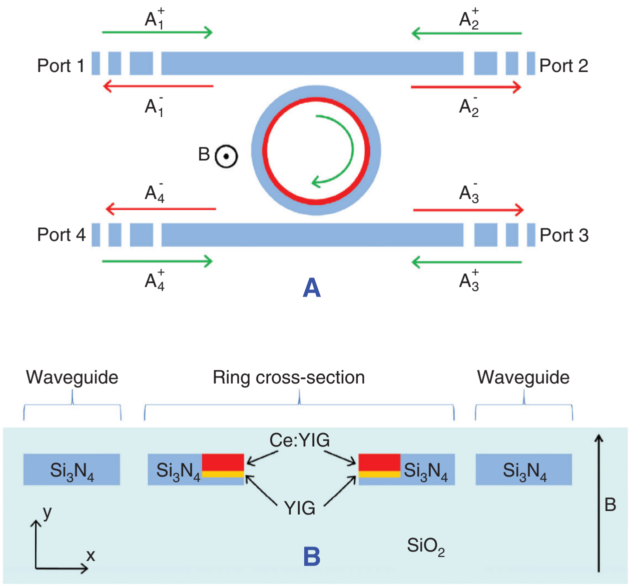

Figure 36 Schematic structure of the TE-mode four-port optical circulator, (A) top view and (B) cross-section.

applying a ~50 Gauss radial magneto-static field with a cylindrical magnet [174], a resonance wavelength split of $\Delta\lambda$~0.325 nm can be reached with the optimal parameters h_{SiN}=200 nm and $h_{Ce:YIG}$ = 175 nm [173], which enables an integrated circulator with a high ER.

6 Conclusion

In this paper, we have reviewed recent progress of on-chip multiplexing technologies and devices for Peta-bps optical interconnect. CWDM technology is potentially a better option than DWDM technology due to the relaxed requirements for the wavelength alignment/control. In order to satisfy the increasing demands, more CWDM channels are needed, which is available since the transparent window for optical waveguides/fibers is large regarding the short transmission distance. The link capacity for a single-wavelength carrier can be enhanced by utilizing the PDM as well as the SDM technologies. Since the planar optical waveguide can maintain the polarization state very well, the PDM technology for on-chip optical interconnects can be simplified greatly because it is not necessary to work with advanced channel coding techniques as well as DSP. By combining these multiplexing technologies to form a kind of multi-dimensional hybrid multiplexing technology, it is possible to achieve hundreds of channels and consequently a huge link capacity as high as Petabps in total. Ultrasmall multiplexers for WDM, PDM as well as SDM have been proposed and demonstrated. However, the channel number is currently still quite limited. It will be desired to achieve more channels, especially for the WDM, and SDM technologies. In addition, in order to realize the multi-dimensional hybrid multiplexing technology, one needs to integrate different types of multiplexer devices on a single chip. Some of these multiplexers are required to be able to deal with not only the fundamental mode but also the higher-order modes, which is not easy and still under exploration. Bidirectional multiplexing technology and devices may be needed to further double the transmission capacity of an optical interconnect link.

Acknowledgements: This project was partially supported by the NSFC (61077040, and 11374263), a 863 project (No. 2011AA010301), Zhejiang provincial grant (Z201121938) of China, and also supported by the Fundamental Research Funds for the Central Universities. The research at UCSB was supported by the EPHI and IPHOD DARPA MTO contracts. The authors thank Sailing He, Zhechao Wang, Xiaowei Guan, Jian Wang, Dan Blumenthal, Nadir Dagli, Di Liang, Jared Bauters, Martijn Heck, Paolo Pintus and Daryl Spencer for insights and conversations.

Received June 15, 2013; accepted October 17, 2013; previously published online November 14, 2013

References

[1] Shacham A, Bergman K, Carloni LP. Photonic networks-on-chip for future generations of chip multiprocessors. IEEE Trans Computers 2008;57:1246–60.
[2] Paniccia MJ. A perfect marriage: optics and silicon. Optik & Photonik 2011;2:34–8.
[3] Ahn J, Fiorentino M, Beausoleil RG, Binkert N, Davis A, Fattal D, Jouppi NP, McLaren M, Santori CM, Schreiber RS, Spillane SM, Vantrease D, Xu Q. Devices and architectures for photonic chip-scale integration. Appl Phys A 2009;95:989–97.
[4] Alduino A, Liao L, Jones MR, Morse M, Kim B, Lo W-Z, Basak J, Koch B, Liu HF, Rong H, Sysak M, Krause C, Saba R, Lazar D, Horwitz L, Bar R, Litski S, Liu A, Sullivan K, Dosunmu O, Na N, Yin T, Haubensack F, Hsieh I-w, Heck J, Beatty R, Park H, Bovington J, Lee S, Nguyen H, Au H, Nguyen K, Merani P, Hakami M, Paniccia M. Demonstration of a High Speed 4-Channel Integrated Silicon Photonics WDM Link with Hybrid Silicon Lasers. in Integrated Photonics Research, Silicon and Nanophotonics and Photonics in Switching, OSA Technical Digest (CD) (Optical Society of America, 2010), paper PDIWI5.

[5] Sandel D, Hinz S, Noé R, Wüst F. Practical 2x10Gbit/s polarization division multiplex transmission system. European Conference on Optical Communication 2000, Munich, Germany, 2000;3:103–5.
[6] Doerr C, Taunay T. Silicon photonics core-, wavelength-, and polarization-diversity receiver. IEEE Photon Tech Lett 2011;3:597–9.
[7] Berdagué S, Facq P. Mode division multiplexing in optical fibers. Appl Opt 1982;21:1950–5.
[8] Randel S, Ryf R, Sierra A, Winzer PJ, Gnauck AH, Bolle CA, Essiambre RJ, Peckham DW, McCurdy A, Lingle R. 6×56-Gb/s mode-division multiplexed transmission over 33-km few-mode fiber enabled by 6×6 MIMO equalization. Opt Express 2011;19:16697–707.
[9] Kawaguchi Y, Tsutsumi K. Mode multiplexing and demultiplexing devices using multimode Interference couplers. Electron Lett 2002;38:1701–2.
[10] Dai D. Silicon mode-(de)multiplexer for a hybrid multiplexing system to achieve ultrahigh capacity photonic networks-on-chip with a single-wavelength-carrier light. in Asia Communications and Photonics Conference, OSA Technical Digest (online) (Optical Society of America, 2012), paper ATh3B.3.
[11] Yadin Y, Orenstein M. Parallel optical interconnects over multimode waveguides. J Lightwave Technol 2006;24:380–6.
[12] Yamada K, Shoji T, Tsuchizawa T, Watanabe T, Takahashi T, Itabashi S. Silicon-wire-based ultrasmall lattice filters with wide free spectral ranges. Opt Lett 2003;28:1663–4.
[13] Jinguji K, Oguma M. Optical Half-Band Filters. J Lightwave Technol 2000;18:252–9.
[14] Oguma M, Kitoh T, Inoue Y, Mizuno T, Shibata T, Kohtoku M, Hibino Y. Compact and low-loss interleave filter employing lattice-form structure and silica-based waveguide. J Lightwave Technol 2004;22:895–902.
[15] Horst F, Green WMJ, Assefa S, Shank SM, Vlasov YA, Offrein BJ. Cascaded Mach-Zehnder wavelength filters in silicon photonics for low loss and flat pass-band WDM (de-) multiplexing. Opt Express 2013;21:11652–8.
[16] Okamoto K. Progress and technical challenge for planar waveguide devices: silica and silicon waveguides. Laser Photon Rev 2011;1–10.
[17] Dragone C. An N×N optical multiplexer using a planar arrangement of two star couplers. IEEE Photon Technol Lett 1991;3:812–4.
[18] Doerr C, Okamoto K. Advances in silica planar lightwave circuits. J Lightwave Technology 2006;24:4763–89.
[19] Dumon P, Bogaerts W, Thourhout DV, Taillaert D, Wiaux V, Beckx S, Wouters J, Baets R. Wavelength-selective components in SOI photonic wires fabricated with deep UV lithography. in Proc. Conf. Group IV Photonics, Hong Kong, Sep. 2004, p. WB5.
[20] Fukazawa T, Ohno F, Baba T. Very compact arrayed-waveguide-grating demultiplexer using Si photonic wire waveguides. Jpn J Appl Phys 2004;43:673–5.
[21] Sasaki K, Ohno F, Motegi A, Baba T. Arrayed waveguide grating of 70×60μm^2 size based on Si photonic wire waveguides. Electron Lett 2005;41:801–2.
[22] Dai D, Liu L, Wosinski L, He S. Design and fabrication of ultrasmall overlapped AWG demultiplexer based on alpha-SOI nanowire waveguides. Electron Lett 2006;42:400–2.
[23] Bogaerts W, Dumon P, Thourhout DV, Taillaert D, Jaenen P, Wouters J, Beckx S, Wiaux V, Baets RG. Compact wavelength selective functions in silicon-on-insulator photonic wires. J Sel Top Quantum Electron 2006;12:1394–401.
[24] Dumon P, Bogaerts W, Thourhout DV, Taillaert D, Baets R, Wouters J, Beckx S, Jaenen P. Compact wavelength router based on a Silicon-on-insulator arrayed waveguide grating pigtailed to a fiber array. Opt Express 2006;14:664–9.
[25] Fang Q, Liow TY, Song JF, Ang KW, Yu MB, Lo GQ, Kwong D-L. WDM multi-channel silicon photonic receiver with 320 Gbps data transmission capability. Opt Express 2010;18: 5106–13.
[26] Bogaerts W, Selvaraja SK, Dumon P, Brouckaert J, De Vos K, Van Thourhout D, Baets R. Silicon-on-insulator spectral filters fabricated with CMOS technology. IEEE J Sel Top Quant Electron 2010;16:33–44.
[27] Dai D, Fu X, Shi Y, He S. Experimental demonstration of an ultra-compact Si-nanowire-based reflective arrayed-waveguide grating (de)multiplexer with photonic crystal reflectors. Opt Lett 2010;35:2594–6.
[28] Shi Y, Fu X, Dai D. Design and fabrication of a 200 GHz Si-nanowire-based reflective arrayed-waveguide grating (de) multiplexer with optimized photonic crystal reflectors. Appl Opt 2010;49:4859–65.
[29] Fu X, Dai D. Ultra-small Si-nanowire-based 400 GHz-spacing 15×15 arrayed-waveguide grating router with microbends. Electron Lett 2011;47:266–8.
[30] Brouckaert J, Bogaerts W, Dumon P, Thourhout DV, Baets R. Planar concave grating demultiplexer fabricated on a nanophotonic silicon-on-insulator platform. J Lightwave Technol 2007;25:1269–75.
[31] Brouckaert J, Bogaerts W, Selvaraja S, Dumon P, Baets R, Thourhout DV. Planar concave grating demultiplexer with high reflective bragg reflector facets. IEEE Photon Technol Lett 2008;20:309–11.
[32] Horst F. Silicon Integrated Waveguide Devices for Filtering and Wavelength Demultiplexing. in Optical Fiber Communication Conference, OSA Technical Digest (CD) (Optical Society of America, 2010), paper OWJ3.
[33] Horst F, Green WMJ, Offrein BJ, Vlasov YA. Silicon-on-insulator echelle grating WDM demultiplexers with two stigmatic points. IEEE Photon Technol Lett 2009;21:1743–5.
[34] Kyotoku BB, Chen L, Lipson M. Broad Band 1 nm Channel Spacing Silicon-on-Insulator Wavelength Division Multiplexer. in Conference on Lasers and Electro-Optics/International Quantum Electronics Conference, OSA Technical Digest (CD) (Optical Society of America, 2009), paper JWA41.
[35] Little BE, Chu ST, Haus HA, Foresi J. Microring resonator channel dropping filters. J Lightwave Technol 1997;15:998–1005.
[36] PopovMiloš A, Barwicz T, Watts MR, Rakich PT, Socci L, Ippen EP, Kärtner FX, Smith HI. Multistage high-order microring-resonator add-drop filters. Opt Lett 2006;31: 2571–3.
[37] Shen H, Khan MH, Fan L, Zhao L, Xuan Y, Ouyang J, Varghese LT, Qi M. Eight-channel reconfigurable microring filters with tunable frequency, extinction ratio and bandwidth. Opt Express 2010;18:18067–76.
[38] Xu F, Poon AW. Silicon cross-connect filters using microring resonator coupled multimode-interference-based waveguide crossings. Opt Express 2008;16:8649–57.
[39] Little BE, Chu ST, Pan W, Kokubun Y. Microring resonator arrays for VLSI photonics. IEEE Photon Technol Lett 2000;12:323–5.

[40] Smit MK, Dam C. Phasar-based WDM-devices: principles, design and applications. IEEE J Select Top Quant Electron 1996;2:236–50.

[41] Khan SN, Dai D, Liu L, Wosinski L, He S. Optimal design for a flat-top AWG demultiplexer by using a fast calculation method based on a Gaussian beam approximation. Opt Commun 2006;262:175–9.

[42] Thourhout D. Silicon Nanophotonics. in Optical Fiber Communication Conference, OSA Technical Digest (CD) (Optical Society of America, 2010), paper OTuB5.

[43] Zortman WA, Trotter DC, Watts MR. Silicon photonics manufacturing. Opt Express 2010;18:23598–607.

[44] Dai D, Shi Y, He S. Comparative study of the integration density for passive linear planar lightwave circuits based on three different kinds of nanophotonic waveguides. Appl Opt 2007;46:1126–31.

[45] Dai D, He S. Ultra-small overlapped arrayed-waveguide grating based on Si nanowire waveguides for dense wavelength division demultiplexing. IEEE J Select Top Quant Electron 2006;12:1301–5.

[46] Dai D, He S. Novel ultracompact Si-nanowire-based arrayed-waveguide grating with microbends. Opt Express 2006;14:5260–5.

[47] Dai D, He S. Novel ultracompact AWG interleaver based on Si-nanowires with spirals. Opt Commun 2008;281:3471–5.

[48] Petalta LG, Bernussi AA, Frisbie S, Gale R, Temkin H. Reflective arrayed waveguide grating multiplexer. IEEE Photons Technol Lett 2003;15:1398–400.

[49] Soole JBD, Amersfoort MR, LeBlanc HP, Rajhel A, Caneau C, Youtsey C, Adesida I. Compact polarisation independent InP reflective arrayed waveguide grating filter. Electron Lett 1996;32:1769–70.

[50] Bernussi AA, Grave de PL, Gorbounov V, Linn JA, Frisbie S, Gale R, Temkin H. Mirror quality and the performance of reflective arrayed-waveguide grating multiplexers. J Lightwave Technol 2004;22:1828–32.

[51] Inoue Y, Himeno A, Moriwaki K, Kawachi M. Silica-based arrayed-wave-guide grating circuit as optical splitter router. Electron Lett 1995;31:726–7.

[52] Liang D, Srinivasan S, Fattal DA, Fiorentino M, Huang Z, Spencer DT, Bowers JE, Beausoleil RG. Teardrop reflector-assisted unidirectional hybrid silicon microring lasers. IEEE Photon Technol Lett 2012;24:1988–90.

[53] Goh T, Suzuki S, Sugita A. Estimation of waveguide phase error in silica-based waveguides. J Lightwave Technol 1997;15:2107–113.

[54] Dai D, He JJ, He S. Elimination of multimode effects in a silicon-on-insulator etched diffraction grating demultiplexer with bi-level taper structure. IEEE J Select Top Quant Electron 2005;11:439–43.

[55] He JJ, Lamontagne B, Ge A, Erickson L, Davies M, Koteles ES. Monolithic integrated wavelength demultiplexer based on a waveguide rowland circle grating in InGaAsP/InP. J Lightwave Technol 1998;16:631–8.

[56] Chen L. Silicon Photonic Integrated Circuits for WDM Technology and Optical Switch. in Optical Fiber Communication Conference/National Fiber Optic Engineers Conference 2013, OSA Technical Digest (online) (Optical Society of America, 2013), paper OW1C.1.

[57] Pinguet T, Analui B, Balmater E, Guckenberger D, Harrison M, Koumans R, Kucharski D, Liang Y, Masini G, Mekis A, Mirsaidi S, Narasimha A, Peterson M, Rines D, Sadagopan V, Sahni S, Sleboda TJ, Song D, Wang Y, Welch B, Witzens J, Yao J, Abdalla S, Gloeckner S, de Dobbelaere P, Capellini G. Monolithically integrated high-speed CMOS photonic transceivers. 2008 5th IEEE International Conference on Group IV Photonics. 17–19, 2008;362–4.

[58] Hansuek L, Tong C, Jiang L, Ki YY, Seokmin J, Oskar P, Kerry JV. Chemically etched ultrahigh-Q wedge-resonator on a silicon chip. Nature Photonics 2012;6:369–73.

[59] Xu Q, Fattal D, Beausoleil RG. Silicon microring resonators with 1.5-μm radius. Opt Express 2008; 6:4309–15.

[60] Prabhu AM, Tsay A, Han Z, Van V. Ultracompact SOI microring add–drop filter with wide bandwidth and wide FSR. IEEE Photon Technol Lett 2009;21:651–3.

[61] Xu Q, Schmidt B, Shakya J, Lipson M. Cascaded silicon micro-ring modulators for WDM optical interconnection. Opt Express 2006;14:9431–5.

[62] Niehusmann J, Vörckel A, Bolivar PH, Wahlbrink T, Henschel W. Ultrahigh-quality-factor silicon-on-insulator microring resonator. Opt Lett 2006;29:2861–3.

[63] Green WMJ, Lee RK, Derose GA, Scherer A, Yariv A. Hybrid InGaAsP-InP Mach-Zehnder racetrack resonator for thermooptic switching and coupling control. Opt Express 2005;13:1651–9.

[64] Chen L, Sherwood-Droz N, Lipson M. Compact bandwidth-tunable microring resonators. Opt Lett 2007;32: 3361–3.

[65] Dai D, He S. Highly sensitive sensor based on an ultra-high-Q Mach-Zehnder interferometer-coupled microring. J Opt Soc Am B 2009;26:511–6.

[66] Wang J, Dai D. Highly sensitive Si nanowire-based optical sensor using a Mach-Zehnder interferometer coupled microring. Opt Lett 2010;35:4229–31.

[67] Dong P, Qian W, Liang H, Shafiiha R, Feng D, Li G, Cunningham JE, Krishnamoorthy AV, Asghari M. Thermally tunable silicon racetrack resonators with ultralow tuning power. Opt Express 2010;18:20298–304.

[68] Dong P, Qian W, Liang H, Shafiiha R, Wang X, Feng D, Li G, Cunningham JE, Krishnamoorthy AV, Asghari M. 1x4 reconfigurable demultiplexing filter based on free-standing silicon racetrack resonators. Opt Express 2010;18:24504–9.

[69] Dong P, Qian W, Liang H, Shafiiha R, Feng N-N, Feng D, Zheng X, Krishnamoorthy AV, Asghari M. Low power and compact reconfigurable multiplexing devices based on silicon microring resonators. Opt Express 2010;18:9852–8.

[70] Almeida VR, Xu Q, Barrios CA, Lipson M. Guiding and confining light in void nanostructure. Opt Lett 2004;29:1209–11.

[71] Wiederhecker GS, Chen L, Gondarenko A, Lipson M. Controlling photonic structures using optical forces. Nature 2009;462:633–6.

[72] Akihama Y, Hane K. Single and multiple optical switches that use freestanding silicon nanowire waveguide couplers. Light Sci Appl 1:e16;doi:10.1038/lsa.2012.16.

[73] Liu B, Shakouri A, Bowers JE. Wide tunable double ring resonator coupled lasers. IEEE Photon Technol Lett 2002;14:600–2.

[74] Dai D. Highly sensitive digital optical sensor based on cascaded high-Q ring-resonators. Opt Express 2009;17:23817–22.

[75] Hu J, Dai D. Cascaded-ring optical sensor with enhanced sensitivity by using suspended Si-nanowires. IEEE Photon Technol Lett 2011;23:842–4.

[76] Kamei S. Recent progress on athermal AWG wavelength multiplexer. in Optical Fiber Communication Conference, OSA Technical Digest (CD) (Optical Society of America, 2009), paper OWO1.
[77] Kamei S, Shibata T, Inoue Y. Compensation for second-order temperature dependence in athermal arrayed waveguide grating realizing wide temperature range oPetation. Photon Technol Lett 2009;21:1695–7.
[78] Maru K, Abe Y. Low-loss, flat-passband and athermal arrayed-waveguide grating multi/demultiplexer. Opt Express 2007;15:18351–6.
[79] Eun-Seok K, Woo-Soo K, Duk-Jun K, Byeong-Soo B. Reducing the thermal dependence of silica-based arrayed waveguide grating using inorganic-organic hybrid materials. IEEE Photon Technol Lett 2004;16:2625–7.
[80] Tanobe H, Kondo Y, Kadota Y, Okamoto K, Yoshikuni Y. Temperature insensitive arrayed waveguide gratings on InP substrates. IEEE Photon Technol Lett 1998;10:235–7.
[81] Wang X, Xiao S, Zheng W, Wang F, Hao Y, Jiang X, Wang M, Yang J. Athermal silicon arrayed waveguide grating with polymer-filled slot structure. Opt Commun 2009;282: 2841–4.
[82] Lee JM, Kim DJ, Kim GH, Kwon OK, Kim KJ, Kim G. Controlling temperature dependence of silicon waveguide using slot structure. Opt Express 2008;16:1645–52.
[83] Zhou L, Okamoto K, Yoo SJB. Athermalizing and trimming of slotted silicon microring resonators with UV sensitive PMMA upper-cladding. Photon Technol Lett 2009;21:1175–7.
[84] Wang L, Bogaerts W, Dumon P, Selvaraja SK, Teng J, Pathak S, Han X, Wang J, Jian X, Zhao M, Baets R, Morthier G. Athermal arrayed waveguide gratings in silicon-on-insulator by overlaying a polymer cladding on narrowed arrayed waveguides. Appl Opt 2012;51:1251–6.
[85] Lee JM, Kim DJ, Ahn H, Park SH, Kim G. Temperature dependence of silicon nanophotonic ring resonator with a polymeric overlayer. J Lightwave Technol 2007;25: 2236–43.
[86] Teng J, Dumon P, Bogaerts W, Zhang H, Jian X, Han X, Zhao M, Morthier G, Baets R. Athermal silicon-oninsulator ring resonators by overlaying a polymer cladding on narrowed waveguides. Opt Express 2009;17:14627–33.
[87] Uenuma M, Motooka T. Design of a temperature independent arrayed waveguide grating on SOI substrates. in 4th IEEE International Conference Group IV Photonics, 2007 (IEEE, 2007), pp. 1–3.
[88] Uenuma M, Motooka T. Temperature-independent silicon waveguide optical filter. Opt Lett 2009;34:599–601.
[89] Huang H, Ho ST, Huang D, Tu Y, Liu W. Design of temperature-independent arrayed waveguide gratings based on the combination of multiple types of waveguide. Appl Opt 2010;49:3025–34.
[90] Vivien L, Laval S, Dumont B, Lardenois S, Koster A, Cassan E. Polarization-independent single-mode rib waveguides on silicon-on-insulator for telecommunication wavelengths. Opt Commun 2002;210:43.
[91] Dai D, He S. Analysis of the birefringence of a silicon-on-insulator rib waveguide. Appl Opt 2004;43:1156.
[92] Chan S, Png C, Lim S, Reed G, Passaro V. Single-mode and polarization-independent silicon-on-insulator waveguides with small cross section. J Lightwave Technol 2005;23:2103.
[93] Xu DX, Cheben P, Dalacu D, Delâge A, Janz S, Lamontagne B, Picard M-J, Ye WN. Eliminating the birefringence in silicon-on-insulator ridge waveguides by use of cladding stress. Opt Lett 2004;29:2384.
[94] Trinh PD, Yegnanarayanan S, Coppinger F, Jalali B. Silicon-on-insulator (SOI) phased-array wavelength multi/demultiplexer with extremely low-polarization sensitivity. IEEE Photon Technol Lett 1997;9:940.
[95] Dai D, He S. Design of a polarization-insensitive arrayed waveguide grating demultiplexer based on silicon photonic wires. Opt Lett 2006;31:1988.
[96] Zou J, Lang T, Wang L, He JJ. Uniform polarization-dispersion compensation of all channels in highly birefringent silicon nanowire-based arrayed waveguide grating. IEEE Photon Technol Lett 2011;23:1787.
[97] Dai D, He S. Optimization of ultracompact polarization-insensitive multimode interference couplers based on SOI nanowire waveguides. IEEE Photon Technol Lett 2006;18:2017.
[98] Wang Z, Dai D, He S. Polarization-insensitive ultrasmall microring resonator design based on optimized si sandwich nanowires. IEEE Photon Technol Lett 2007;19:1580.
[99] Shi Y, Anand S, He S. Design of a polarization insensitive triplexer using directional couplers based on submicron silicon rib waveguides. J Lightwave Technol 2009;27:1443.
[100] Shi Y, Anand S, He S. A polarization-insensitive 1310/1550-nm demultiplexer based on sandwiched multimode interference waveguides. IEEE Photon Technol Lett 2007;19:1789.
[101] Fukuda H, Yamada K, Tsuchizawa T, Watanabe T, Shinojima H, Itabashi S. Silicon photonic circuit with polarization diversity. Opt Express 2008;16:4872–80.
[102] Dai D, Liu L, Gao S, Xu D, He S. Polarization management for silicon photonic integrated circuits. Laser Photon Rev 2013;7:303–28.
[103] Barwicz T, Watts M, Popovic M, Rakich PT, Socci L, Kärtner FX, Ippen EP, Smith HI. Polarization-transparent microphotonic devices in the strong confinement limit. Nature Photon 2007;1:57–60.
[104] Pfau T, Peveling R, Hauden J, Grossard N, Porte H, Achiam Y, Hoffmann S, Ibrahim SK, Adamczyk O, Bhandare S, Sandel D, Porrmann M, Noe R. Coherent digital polarization diversity receiver for real-time polarization-multiplexed QPSK transmission at 2.8 Gb/s. IEEE Photon Technol Lett 2007;19:1988–90.
[105] Sansoni L, Sciarrino F, Vallone G, Mataloni P, Crespi A, Ramponi R, Osellame R. Polarization entangled state measurement on a chip. Phys Rev Lett 2010;105:200503.
[106] Hong JM, Ryu HH, Park SR, Jeong JW, Gol LS, Lee E-H, Park S-G, Woo D, Kim S, Beom-Hoan O. Design and fabrication of a significantly shortened multimode interference coupler for polarization splitter application. IEEE Photon Technol Lett 2003;15:72–4.
[107] Jiao Y, Dai D, Shi Y, He S. Shortened polarization beam splitters with two cascaded multimode interference sections. IEEE Photon Technol Lett 2009;21:1538–40.
[108] Rahman BMA, Somasiri N, Themistos C, Grattan KTV. Design of optical polarization splitters in a single-section deeply etched MMI waveguide. Appl Phys B 2001;73:613–8.
[109] Katigbak A, Strother JF, Lin J. Compact silicon slot waveguide polarization splitter. Opt Eng 2009;48:080503.

[110] Yang BK, Shin SY, Zhang DM. Ultrashort polarization splitter using two-mode interference in silicon photonic wires. IEEE Photon Technol Lett 2009;21:432–4.

[111] Kiyat I, Aydinli A, Dagli N. A compact silicon-on-insulator polarization splitter. IEEE Photon Technol Lett 2005;17:100–2.

[112] Augustin LM, van der Tol JJGMR. Hanfoug R, De Laat, Wim JM, Van de Moosdijk, Michael JE, Dijk Paul WL van, Oei YS, Smit MMK. A single etch-step fabrication-tolerant polarization splitter. J Lightwave Technol 2007;25:740–6.

[113] Xiao J, Liu X, Sun X. Design of a compact polarization splitter in horizontal multiple-slotted waveguide structures. Jap J Appl Phys 2008;47:3748–54.

[114] Tu XG, Ang SSN, Chew AB, Teng J, Mei T. An ultracompact directional coupler based on GaAs cross-slot waveguide. IEEE Photon Technol Lett 2010;22:1324–6.

[115] Yamazaki T, Aono H, Yamauchi J, Nakano H. Coupled Waveguide polarization splitter with slightly different core widths. J Lightwave Technol 2008;26:3528–33.

[116] Yue Y, Zhang L,Yang JY, Beausoleil RG, Willner AE. Silicon-on-insulator polarization splitter using two horizontally slotted waveguides. Opt Lett 2010;35:1364–6.

[117] Fukuda H, Yamada K, Tsuchizawa T, Watanabe T, Shinojima H, Itabashi S. Ultrasmall polarization splitter based on silicon wire waveguides. Opt Express 2006;14:12401–8.

[118] Komatsu M, Saitoh K, Koshiba M. Design of miniaturized silicon wire and slot waveguide polarization splitter based on a resonant tunneling. Opt Express 2009;17:19225–33.

[119] Soldano LB, Vreede AH, de Smit MK, Verbeek Metaal BHEG, Groen FH. Mach-Zehnder interferometer polarization splitter in InGaAsP-InP. IEEE Photon Technol Lett 1994;6:402–5.

[120] Liang TK, Tsang HK. Integrated PBS in high index contrast silicon-on-insulator waveguides. IEEE Photon Technol Lett 2005;17:393–5.

[121] Augustin LM, Hanfoug R, Van der Tol JJGM, De Laat WJM, Smit MK. A compact integrated polarization splitter/converter in InGaAsP–InP. IEEE Photon Technol Lett 2007;19:1286–8.

[122] Shi Y, Dai D, He S. Proposal for an ultra-compact PBS based on a photonic crystal-assisted multimode interference coupler. IEEE Photon Technol Lett 2007;19:825–7.

[123] Tang Y, Dai D, He S. Proposal for a grating waveguide serving as both a polarization splitter and an efficient coupler for silicon-on-insulator nanophotonic circuits. IEEE Photon Technol Lett 2009;21:242–4.

[124] Wang Z, Tang Y, Zhu N, Wosinski L, Dai D, Westergren U, He S. Experimental demonstration of an ultracompact polarization beam splitter based on a bidirectional grating coupler. Proc SPIE 2009;7631:1–2.

[125] Shi Y, Shahid N, Li M, Berrier A, He S, Anand S. Experimental demonstration of an ultracompact polarization beamsplitter based on a multimode interference coupler with internal photonic crystals. Opt Eng 2010;49:060503.

[126] Ao X, Liu L, Wosinski L, He S. Polarization beam splitter based on a two-dimensional photonic crystal of pillar type. Appl Phys Lett 2006;89:171115.

[127] Ye WN, Xu DX, Janz S, Waldron P, Cheben P, Tarr NG. Passive broadband silicon-on-insulator polarization splitter. Opt Lett 2007;32:1492–4.

[128] Huang QZ, Yu YD, Yu JZ. Design and realization of a microracetrack resonator based polarization splitter in silicon-on-insulator. J Opt A 2009;11:015506.

[129] Dai D. Silicon polarization beam splitter based on an asymmetrical evanescent coupling system with three optical waveguides. J Lightwave Technol 2012;30:3281–7.

[130] Dai D, Bowers JE. Novel ultra-short and ultra-broadband polarization beam splitter based on a bent directional coupler. Opt Express 2011;19:18614–20.

[131] Wang J, Liang D, Tang Y, Dai D, Bowers JE. Realization of an ultra-short silicon polarization beam splitter with an asymmetrical bent directional coupler. Opt Lett 2013; 38:4–6.

[132] Dai D, Wang Z, Bowers JE. Ultrashort broadband polarization beam splitter based on an asymmetrical directional coupler. Opt Lett 2011;36:2590–2.

[133] Lin S, Hu J, Crozier KB. Ultracompact, broadband slot waveguide polarization splitter. Appl Phys Lett 2011;98:151101.

[134] Lou F, Dai D, Wosinski L. Ultracompact polarization beam splitter based on a dielectric–hybrid plasmonic–dielectric coupler. Opt Lett 2012;37:3372–4.

[135] Chee J, Zhu S, Lo GQ. CMOS compatible polarization splitter using hybrid plasmonic waveguide. Opt Express 2012;20:25345–55.

[136] Feng N, Sun R, Kimerling L, Michel J. Lossless strip-to-slot waveguide transformer. Opt Lett 2007;32:1250–2.

[137] Dai D, He S. A silicon-based hybrid plasmonic waveguide with a metal cap for a nano-scale light confinement. Opt Express 2009;17:16646–53.

[138] Guan X, Wu H, Shi Y, Wosinski L, Dai D. Ultra-compact and broadband polarization beam splitter utilizing the evanescent coupling between a hybrid plasmonic waveguide and a silicon nanowire. Opt Lett 2013;38:3005–8.

[139] Shani Y, Alferness R, Koch T, Koren U, Oron M, Miller BI, Young MG. Polarization rotation in asymmetric periodic loaded rib waveguides. Appl Phys Lett 1991;59:1278–80.

[140] van del Tol JJGM, Hakimzadeh F, Pedersen JW, Li D, van Brug H. A new short and low-loss passive polarization converter on InP. IEEE Photon Technol Lett 1995;7:32–4.

[141] Obayya S, Rahman B, Grattan K, El-Mikati H. Beam propagation modeling of polarization rotation in deeply etched semiconductor bent waveguides. IEEE Photon Technol Lett 2001;13:681–3.

[142] Obayya S, Rahman, B, Grattan K, El-Mikati H. Improved design of a polarization converter based on semiconductor optical waveguide bends. Appl Opt 2001;40:5395–401.

[143] Holmes B, Hutchings D. Realization of novel low-loss monolithically integrated passive waveguide mode converters. IEEE Photon Technol Lett 2006;12:43–5.

[144] Daryl MB, Michele M, Thomas FK. Compact polarization rotators for integrated polarization diversity in InP-based waveguides. Opt Lett 2007;32:2176–8.

[145] Huan Z, Scarmozzino R, Nagy G, Steel J, Osgood RM. Realization of a compact and single-mode optical passive polarization converter. IEEE Photon Technol Lett 2000;12:317–9.

[146] Deng H, Yevick DO, Brooks C, Jessop PE. Design rules for slanted-angle polarization rotators. IEEE J Lightwave Technol 2005;23:432–45.

[147] Deng H, Yevick DO, Brooks C, Jessop PE. Fabrication tolerance of asymmetric silicon-on-insulator polarization rotators. J Opt Soc Am A 2006;23:1741–5.

[148] Brooks C, Jessop PE, Deng Yevick HDO, Tarr G. Passive silicon-on-insulator polarization-rotating waveguides. Opt Eng 2006;45:044603.

[149] Velasco AV, Calvo ML, Cheben P, Ortega-Moñux A, Schmid JH, Ramos CA, Fernandez IM, Lapointe J, Vachon M, Janz S, Xu D-X. Ultracompact polarization converter with a dual subwavelength trench built in a silicon-on-insulator waveguide. Opt Lett 2012;37:365–7.

[150] Zhang J, Yu M, Lo G, Kwong DL. Silicon waveguide based mode-evolution polarization rotator. IEEE J Sel. Top. Quantum Electron 2010; 16:53–60.

[151] Wang Z, Dai D. Ultrasmall Si-nanowire-based polarization rotator. J Opt Soc Am B 2008;25:747–53.

[152] Vermeulen D, Selvaraja S, Verheyen P, Absil P, Bogaerts W, Van Thourhout D, Roelkens G. Silicon-on-insulator polarization rotator based on a symmetry breaking silicon overlay. IEEE Photon Technol Lett 2012;24:482–4.

[153] Dai D, Bowers JE. Novel concept for ultracompact polarization splitter-rotator based on silicon nanowires. Opt Express 2011;19:10940–9.

[154] Liu L, Ding Y, Yvind K, Hvam JM. Silicon-on-insulator polarization splitting and rotating device for polarization diversity circuits. Opt Express 2011;19:12646–51.

[155] Vermeulen D, Acoleyen K, Ghosh S, Selvaraja WADD, Cort NA, Yebo E, Hallynck KD, Vos P, Debackere PP, Dumon P, Bogaerts W, Roelkens G, Thourhout DY, Baets R. Efficient tapering to the fundamental Quasi-TM mode in asymmetrical waveguides. in Proc. European Conference on Integrated Optics, 2010, pp. 1–2.

[156] Dai D, Tang Y, Bowers JE. Mode conversion in tapered submicron silicon ridge optical waveguides. Opt Express 2012;20:13425–39.

[157] Liang D, Fiorentino M, Okumura T, Chang HH, Spencer DT, Kuo Y-H, Fang AW, Dai D, Beausoleil RG, Bowers JE. Electrically-pumped compact hybrid silicon microring lasers for optical interconnects. Opt Express 2009;17:20355–64.

[158] Saffman M, Anderson DZ. Mode multiplexing and holographic demultiplexing communication channels on a multimode fiber. Opt Lett 1991;16:300–2.

[159] Doerr C. Proposed architecture for MIMO optical demultiplexing using photonic integration. IEEE Photon Tech Lett 2011;23:1573–5.

[160] Uematsu T, Ishizaka Y, Kawaguchi Y, Saitoh K, Koshiba M. Design of a compact two-mode multi/demultiplexer consisting of multi-mode interference waveguides and a wavelength insensitive phase shifter for mode-division multiplexing transmission. J Lightwave Technol 2012;30:2421–6.

[161] Gabrielli LH, Liu D, Johnson SG, Lipson M. On-chip transformation optics for multimode waveguide bends. Nature Commun 2012;3:1217.

[162] Bagheri S, Green WMJ. Silicon-on-insulator mode-selective add-drop unit for on-chip mode-division multiplexing. The 6th IEEE International Conference on Group IV Photonics (GFP '09), 2009;166–168.

[163] Greenberg M, Orenstein M. Mode add drop for optical interconnects based on adiabatic high order mode couplers. Quantum Electronics and Laser Science Conference (QELS '05), 2005;2:942–4.

[164] Dai D, Wang J, Shi Y. Silicon mode (de)multiplexer enabling high capacity photonic networks-on-chip with a single-wavelength-carrier light. Opt Lett 2013;38:1422–4.

[165] Lee LW, Ophir N, Chen C, Gabrielli LH, Poitras CB, Bergman K, Lipson M. Simultaneous mode and wavelength division multiplexing on-chip. arXiv:1306.2378, 24 July 2013.

[166] Bogaerts W, Selvaraja SK. Compact single-mode silicon hybrid rib/strip waveguide with adiabatic bends. IEEE Photon J 2011;3:422–32.

[167] Batten C, Joshi A, Orcutt J, Khilo A, Moss B, Holzwarth C, Popovic M, Hanqing L, Smith HI, Hoyt J, Kartner F, Ram R, Stojanovic V, Asanovic K. Building many-core processor-to-dram networks with monolithic CMOS silicon photonics. IEEE Micro 2009;29:8–21.

[168] Plant DV, Venditti MB, Laprise E, Faucher J, Razavi K, Chateauneuf M, Kirk AG, Ahearn JS. 256-Channel bidirectional optical interconnect using VCSELs and photodiodes on CMOS. J Lightwave Technol 2001;19: 1093–104.

[169] Doany FE, Schow CL, Baks CW, Kuchta DA, Pepeljugoski P, Schares L, Budd R, Libsch F, Dangel R, Horst F, Offrein BJ, Kash JA. 160Gb/s Bidirectional polymer-waveguide board-level optical interconnects using CMOS-based transceivers. IEEE Trans Advanced Packaging 2009;32:345–59.

[170] Schow CL, Doany FE, Baks C, Kwark YH, Kuchta DM, Kash JA. A single-chip CMOS-based parallel optical transceiver capable of 240 Gb/s bi-directional data rates. J Lightwave Technol 2009;27:915–29.

[171] Tai K, Chang B, Chen J, Mao CH, Ducellier T, Xie J, Mao L, Wheeldon J. Wavelength-interleaving bidirectional circulators. IEEE Photon Technol Lett 2001;13:320–2.

[172] Pintus P, Andriolli N, Pasquale FD, Bowers JE. Integrated crosstalk-free active optical link for WDM bidirectional interleaved communication. IEEE Optical Interconnects, Santa Fe, New Mexico, May 5th–8th, 2013.

[173] Pintus P, Pasquale FDi, Bowers JE. Integrated TE and TM optical circulators on ultra-low-loss silicon nitride platform. Opt Express 2013;21:5041–52.

[174] Tien MC, Mizumoto T, Pintus P, Kromer H, Bowers JE. Silicon ring isolators with bonded nonreciprocal magneto-optic garnets. Opt Express 2011;19:11740–5.